UK UNCLASSIFIED
UNLIMITED

DRA TM (AWE) 91013

October 1991

Copy No.

Electronic Warfare Systems Department

DEFENCE RESEARCH AGENCY
Portsdown, Portsmouth, Hants PO6 4AA

THE APPLICATION OF SPACEBORNE SYNTHETIC APERTURE RADAR IN THE MARITIME ENVIRONMENT

by C J Condley

DRA TM (AWE) 91013

Technical Memorandum

UNLIMITED
UK UNCLASSIFIED

CONDITIONS OF RELEASE

0146168

317257

****

DRIC U

****

DRIC Y

Reports quoted are not necessarily available to members of the public or to commercial organisations.

DISCLAIMER NOTICE

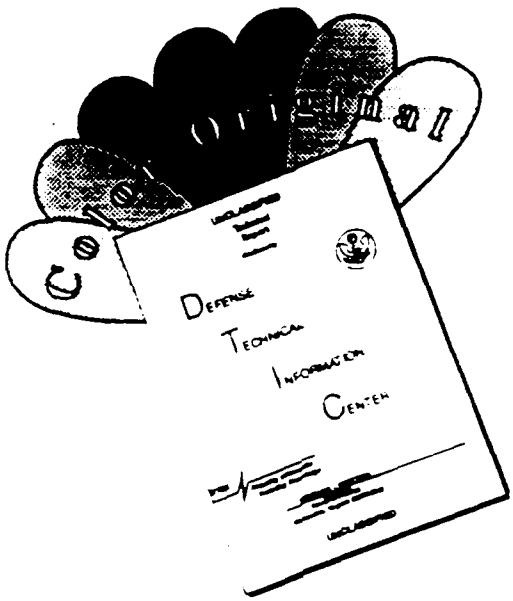

THIS DOCUMENT IS BEST QUALITY AVAILABLE. THE COPY FURNISHED TO DTIC CONTAINED A SIGNIFICANT NUMBER OF COLOR PAGES WHICH DO NOT REPRODUCE LEGIBLY ON BLACK AND WHITE MICROFICHE.

DRA TM (AWE) 91013
October 1991

The Application of Spaceborne Synthetic Aperture Radar in the Maritime Environment

by C J Condley

Approved for release

G.W. Whalley

Head, Electronic Warfare Systems Department

ABSTRACT

A review of the principles of spaceborne Synthetic Aperture Radar (SAR) is given, and its application in the maritime environment is discussed, with reference to several specific systems. The requirement for calibration is discussed, as are some of the more advanced techniques expected to be incorporated in future missions. The paper was written as a dissertation submitted in partial fulfillment of the requirements for the award of an MSc degree in Microwave Solid State Physics undertaken in the Department of Applied Physics and Physical Electronics, University of Portsmouth.

DEFENCE RESEARCH AGENCY
Portsdown, Portsmouth, Hants PO6 4AA

University of Portsmouth
King Henry I Street, Portsmouth PO1 2DZ

TABLE OF CONTENTS

1. WHAT IS SYNTHETIC APERTURE RADAR (SAR) ?

In the very broadest of terms, Synthetic Aperture Radar (SAR) is a coherent imaging radar that takes advantage of platform motion to achieve very high resolution in the along track (cross-range or azimuth) direction. Complementary high resolution in the across track (range) direction is usually achieved by the utilization of conventional pulse compression techniques, although this is not an absolute requirement and an important exception to this general principle is cited by a specific example later. The technique of SAR is not new, in fact the principle was patented by Carl Wiley of the Goodyear Aircraft Corporation in August 1954 [1], and he is credited as having first reported the SAR principle even earlier, in 1951. However, it was not until 1978 that an experimental spaceborne SAR was deployed, in the shape of the NASA/JPL SEASAT mission. The primary objective of the SAR experiment on the SEASAT mission was threefold; to obtain radar imagery of ocean wave patterns in deep oceans, to obtain ocean wave patterns and water-land interaction data in coastal regions and to obtain radar imagery of sea and fresh water ice and snow cover [2]. Although eventually of only ninety eight days operational duration, due to a spacecraft power supply short circuit, this first spaceborne SAR mission was considered to be a great success, leading the way to much more ambitious projects which will be described later.

SAR is based on the generation of an effective long antenna by signal processing means rather than by the use of a physically long antenna. SAR achieves its high azimuth resolution by taking advantage of the motion of the radar platform to translate a single antenna element to take up sequential positions along a line. At each of these positions, a radar signal is transmitted, and the amplitude and phase of the returned radar signal in response to that transmission are stored, figure 1. After the radiating element has traversed a distance L_e, the signals that have been stored resemble the signals that would have been received by the elements of an actual linear array of length L_e. Consequently, if the stored signals are processed in a similar way to those from an actual linear array, the performance of a long effective antenna aperture can be synthesised. For the spaceborne SAR case, the dimensions of the synthesised antenna can exceed the physical dimensions of the real antenna by many times, and can be as great as several kilometres. For a spaceborne SAR, the antenna is usually arranged so as to be side looking with respect to the platform's orbital motion vector and it is this platform motion that carries the radiating element to each of the positions corresponding to the positions of elements in a linear array. These array positions are the positions of the real antenna at the times of transmission and reception of the radar signals.

The returned radar signals can be processed in two ways, leading to two conditions for along track resolution. If the signals received at the synthetic array are coherently integrated with no attempt to alter their phase before integration, the SAR is said to be unfocused. This lack of phase adjustment imposes an upper limit on the length of the synthetic aperture that can be generated. This limit is determined by the far field of the synthetic aperture; that is by the need to restrict the aperture size so that the phase front associated with it can be considered as a plane wave. This maximum length for the synthetic aperture for any given target range occurs when the two-way distance from the target to the centre of the synthetic aperture differs by $\lambda/4$ from the distance between the target and the aperture extremities. In figure 2, R represents the target range to the synthetic aperture of maximum length L_e, such that the difference between this and the target range to the aperture extremity does not exceed $\lambda/8$. It can be seen that, by Pythagoras, the maximum length of the synthetic aperture is given by; $L_e = \sqrt{R\lambda}$. It follows that the along track resolution of such a system is given by; $\delta_a = \sqrt{(R\lambda)/2}$. Hence, the along track resolution for an unfocused SAR is range and frequency dependent.

The limit on resolution imposed on the SAR due to the requirement for operation in the far field can be overcome by correcting the received signal for the curvature of the wave front experienced when the target is within this range. At each element of the synthetic aperture antenna, a phase correction, $\Delta\phi = 2\pi x^2/R\lambda$, proportional to the element's distance from the centre of the array, is applied. Note that a different correction must be applied for each range, and when this correction is applied at each element of the synthetic array, the aperture is said to be focused at that range, and all the received signals from a target are in phase. The angular resolution when the antenna is focused in the Fresnel region is equivalent to that in the far field. Hence the along track resolution of the focused synthetic aperture with $L_e = R\lambda/D$ is $\delta_a = R\theta_S = D/2$ where D is the length of the real antenna and where θ_S is the beamwidth of the synthetic aperture antenna of effective length L_e, and is equal to $\lambda/2L_e$. So, the along track resolution of the focused SAR

is range and frequency independent, and relies solely on the length of the real antenna [3].

A summary of along track resolution for both types of SAR, as a function of range, is given in figure 3, together with that for a conventional radar for comparison. The scales are arbitrary for the general case, since real scales will be dependent on radar parameters. The spaceborne SARs considered in the remainder of this dissertation are all of the fully focused type.

Because SAR is a coherent imaging system, the surface roughness, at the scale of the radar wavelength, produces a random interference pattern in the resulting image. This speckle effect can be reduced by the technique of multiple-look processing [4]. In this technique, several independent images of the same area, which are produced by using different portions of the synthetic aperture, are averaged together to produce a smoother image. However, the implication of this improvement in image quality is a degradation in resolution. The number of independent images averaged is usually referred to as the number of looks. The resultant size of the effective resolution cell is directly proportional to the number of looks. So, for a focused SAR, the effective resolution for multi-look processing becomes $\delta_a = nD/2$, where n is the number of independent looks. Consequently, there is a trade-off between image quality and the absolute resolution of the image. The SAR imagery presented in this dissertation has all been produced using multi-look processing.

For complementary resolution in the range direction, conventional pulse compression techniques are usually employed. Assuming pulse compression to be used, then the range resolution for a spaceborne SAR is given by; $\delta_r = c\tau_p/2\cos\phi$, where c = velocity of EM radiation, τ_p = compressed pulse width and ϕ = depression angle (90°-incidence angle).

In the SAR technique, range-Doppler imaging is employed to form the high resolution image. The Doppler information in the returned radar echo is used simultaneously with the time delay information to generate a high resolution image of the surface being illuminated by the radar. The radar is most often arranged to look to one side of the platform to eliminate left-right ambiguities and perpendicular to its motion vector. It transmits pulses of coherent electromagnetic energy towards the surface of interest. Points equidistant, and hence at equal time delay, from the radar are located on successive concentric spheres. The intersection of these spheres with a flat surface gives a series of concentric circles centred at the nadir point. The backscatter echoes from objects along any particular circle will have a well defined time delay but different Doppler characteristics. Points distributed on co-axial cones, with the motion vector as the axis and the radar as the apex, provide identical Doppler shifts of the returned radar echo but with different delays. The intersection of these cones with a flat surface gives a family of hyperbolae. Objects on any particular hyperbola will provide equi-Doppler returns. Thus if the time delay and Doppler shift information in the returned radar echoes are processed simultaneously, the illuminated surface can be divided into a co-ordinate system of concentric circles and co-axial hyperbolae, figure 4, and each point on the surface will have a unique location in time/Doppler space, identified by a specific time delay and a specific Doppler shift.

The brightness that is assigned to any specific pixel in the image is proportional to the returned radar echo energy contained in the time delay bin and the Doppler bin, which corresponds to the equivalent point on the surface being imaged. The resolution of the imaging system is thus dependent on the measurement accuracy of the differential time delay and differential Doppler (or phase) between two neighbouring points on the surface.

In practice, the situation is more complex than the idealised descriptions above. The radar transmits a pulsed signal in order to obtain the time delay information. To obtain the Doppler information unambiguously, the echoes from many successive pulses are required with a pulse repitition frequency which meets the Nyquist sampling criterion. Thus, as the moving platform passes over a particular region, the received echoes contain a complete Doppler history and range change history for each point on the surface that is illuminated. These range and Doppler histories are then processed to uniquely identify each point on the surface and to generate the image. Consequently, a very large number of operations are required to generate each pixel in the image.

There are important constraints on one particular radar parameter, namely the pulse repitition frequency or PRF, which affect the performance of the SAR. There will be an ambiguity in the response if the PRF is so high that return signals from two successive

transmitted pulses arrive simultaneously at the receiver. This is known as range ambiguity. Conversely, if the PRF is so low that the return is not sampled at the Nyquist rate, there will be Doppler azimuth ambiguity. The upper limit on the PRF is determined by the SAR geometry, such that a situation in which returned echoes from the far edge of the beam arrive at the receiver simultaneously with those from the near edge is avoided. The lower limit on the PRF is imposed by the requirement that the PRF must equal or exceed the maximum Doppler shift of the returned signals. Targets at the centre of the broadside beam will return signals with zero Doppler shift. Targets ahead of broadside will be characterised by a positive Doppler shift and those behind by a negative Doppler frequencies. If the return of a target is shifted in frequency by an amount equal to the PRF, the receiver will be unable to distinguish the pulsed return signal from that of a target on broadside. Thus, the PRF must be sufficiently high to exceed the maximum Doppler shift of targets located at the edges of the beam.

The data gathered by the SAR may be processed in one of a number of ways to form the final image [5]. Historically, the first technique used to process SAR data was the utilisation of Fourier optical methods. Optical processing is a mature technology and is relatively simple to implement. In addition, it is comparitively cheap and, although not "real-time", can produce end results in a reasonably short time. However, the results are generally of low resolution and the methods are unsuited for the generation of precision digital products. Consequently there has been a drive to develop SAR processors using wholly digital techniques. Usually, special purpose hardware systems are used for SAR data processing. Such architectures have the potential of being very fast, approaching real-time operation in some cases. However, they are difficult to construct and maintain and require considerable computing facilities. The most recent development in SAR processors is for exclusively software processors taking advantage of the recent steps forward in micro/mini-computer technology and array processors. Such a SAR processor may take hours, or even days, to process a scene, but is simple to implement and modify and is cheap compared with a dedicated hardware system [6]. Consequently, the choice of SAR processor will be a compromise between cost, timeliness of the required output and the required precision of the output product. The SAR imagery presented in this dissertation is, with one exception, digitally processed, indicating that optical methods of processing have not been wholly supplanted by digital techniques.

2. WHY IS SAR IMPORTANT IN THE MARITIME ENVIRONMENT ?

In maritime applications, SAR posesses one unique characteristic, absent in other spaceborne imaging techniques (eg. optical or thermal I.R.). Because it is an active sensor, SAR has the capability to acquire its high resolution images at any time of the day or night and regardless of the prevailing cloud cover. This particular characteristic makes the SAR an essential tool for monitoring the oceans because of the dynamic nature of the features of the ocean surface and the presence of atmospheric phenomena often associated with many ocean surface features [7].

The image generated by the SAR sensor is representative of the backscatter characteristics of the surface being illuminated. In the case of the ocean, the backscatter is controlled by the small scale surface topography; the short gravity waves and capillary waves which scatter the radar energy by the Bragg scattering mechanism, and the local tilt of the surface, which is due to the presence of large waves and swells. Thus, the SAR is capable of imaging phenomena that affect the surface roughness, either directly or indirectly. Typical of such phenomena are: surface waves, internal waves, currents, weather fronts, wind or oil slicks, eddies and man-made features. Some of these phenomena will be discussed, in detail, later. A particularly important phenomenon that affects the surface roughness in an indirect way is sea bottom topography. SAR images of shallow sea areas show features that closely correspond to bathymetric charts of the sea bottom. This cannot be direct imaging of the sea bottom, as the radar waves do not penetrate the surface sufficiently for this to take place. The most likely interpretation of this phenomenon is that the change in thickness of the water column modulates the velocity of the near-surface current, which in turn modulates the surface roughness, which, as has already been discussed, is the principal physical parameter that the SAR is sensing [7]. Thus, indirectly, the radar image reflects the sea bottom topography. Man-made features in ocean images are restricted to ships, sometimes with associated wake features, and oil/gas installations. Such features appear as bright point targets in the SAR image.

Two typical images from SEASAT are shown in figures 5 and 6, and they illustrate a number of the phenomena referred to above. The first is of the Western Atlantic Ocean off the coast of Florida near Cape Canaveral, which was acquired on 25 July 1978. Several ships can be seen, together with their associated wakes. The other bright features present in the image are associated with internal wave patterns. The second image is of the Solent and was acquired on 2 September 1978. A number of features, corresponding to the sea bottom are evident, particularly to the south east of the Isle of Wight, also visible are the effects of the ebbing tide in Spithead, particularly around No Man's Land Fort. Both of these images have been digitally processed and are multi-look images. In the case of both images, the azimuth resolution is approximately 24 metres at three looks and the range resolution is approximately 22 metres.

3. EXAMPLES OF SPACEBORNE SAR

Three examples of spaceborne SAR will be described, corresponding to the first generation with SEASAT, the current "state-of-the-art" with ERS-1 and an interesting contrast to Western technology in the shape of the Soviet ALMAZ.

The NASA SEASAT mission was launched on 28 June 1978 from Vandenburg AFB, Ca. and was dedicated to studying the oceans. It was the first spacecraft to carry a SAR into orbit, figures 7 and 8. The principal characteristics of the SAR are given below in table 1.

Frequency	1.275 GHz
Wavelength	23.5 cm
Pulse length	33.4 μs
Bandwidth	19 MHz
PRF	1555 Hz ± 14%
Peak power	1 kW
Polarization	HH
Swath width	100 km
Incidence angle	23° ± 3°
Resolution	25 m x 25 m
Looks	4

Table 1 : SEASAT SAR Parameters

In the event, the mission lasted only one hundred and five days, of which the SAR was operational for only ninety eight days. On 10 October 1978, a massive short circuit developed at the slip rings between the solar array and the spacecraft power distribution bus and so prematurely curtailled the mission.

The SEASAT SAR was a focused SAR consisting of five sub-systems; the spacecraft radar antenna, the spacecraft radar sensor, a spacecraft-to-ground data link, a ground data recorder and formatter and the ground data processor. The antenna of the SEASAT SAR is unique among those described in this dissertation in that it was a microstrip array of eight paneis, fed by a corporate-feed network. It had a solid state transmitter which generated a nominal peak power of 800 W with a linear frequency modulation, derived from a stable local oscillator (STALO). The signal returned from targets and a fraction of the radar STALO were combined and transmitted to a ground station by an analogue data link. At the ground station, a demodulator recovered the radar sensor STALO and radar return signal. The synchronously demodulated video signal thus recovered was then converted into digital form by the radar data recorder and formatter sub-system. On analogue-to-digital conversion, the signal was buffered and recorded by a high density magnetic tape recorder. The radar data processor subsequently converted the digital recorded data into a two-dimensional map of the radar cross section of the area illuminated by the antenna [2]. The antenna dimensions were approximately 11 metres by 2 metres.

Although the original rationale of deploying a SAR on board SEASAT was its potential to monitor the surface wave field of the ocean and polar sea ice, the resulting imagery revealed

the much wider range of phenomena as listed above. The success of the SAR mission proved the application and utility of SAR in the maritime environment and has led on to a number of other missions, both undertaken and scheduled. Direct follow-ons from SEASAT were the two SARs carried on the U.S. space shuttle. These missions, SIR (Shuttle Imaging Radar) -A in 1981 and SIR-B in 1984 used hardware very similar to that deployed on SEASAT.

The bulk of high quality data available to date is from the SEASAT mission with a limited contribution from the SIR missions. Indeed, results are still being obtained from SEASAT data, more than a decade after the demise of the satellite.

The next major development in spaceborne SAR is the European Space Agency's (ESA) ERS-1 (European Remote-sensing Satellite) mission. ERS-1 was launched, after some delay, on 16 July 1991 by Ariane-4 from the ESA launch complex at Kourou, French Guiana. The spacecraft, figures 9 and 10, carries a multi-function Active Microwave Instrument (AMI), one mode of which is a SAR image mode. The principal parameters of this instrument mode are given in table 2 below [8,9].

Frequency	5.3 GHz
Wavelength	5.7 cm
Pulse length	37.1 ± 0.05 μs
Bandwidth	15.5 ± 0.06 MHz
PRF	1640 - 1720 Hz
Peak power	4.8 kW
Polarization	VV
Swath width	100 km
Incidence angle	23° ± 2.9°
Resolution	≤ 30 m (along track), ≤ 26.3 m (range)
Looks	6

Table 2 : ERS-1 AMI SAR Mode Parameters

In SAR image mode, the AMI transmitter I.F. section generates a linearly chirped pulse by applying a short pulse to a dispersive SAW delay line. An up-converter converts this linear frequency modulated I.F. pulse to the radar R.F. and it is then amplified to the level required for the input of the high power amplifier (HPA). The HPA consists of power conditioner unit, a travelling wave tube amplifier (TWT), an output isolator and an output filter. The output signal is then fed to the SAR antenna via a switching matrix. Unlike SEASAT, the SAR antenna of ERS-1 is of slotted waveguide design, constructed from metallised carbon fibre reinforced plastic, and has a radiating area of 10 metres by 1 metre, divided into five panels. Radar returns are fed to the I.F. section via the switching matrix and a down-converter. In the SAR modes, range compression can be commanded to take place on-board the spacecraft. In this case, the return signals are switched to an inverse dispersive SAW delay line, whose output is then fed to the SAR processor. The SAR processor filters the signal and down-converts it to baseband. After analogue-to-digital conversion, auxiliary data are added, the data are then buffered and transferred to the Instrument Data-Handling and Telemetry (IDHT) sub-system for transmission to the ground [10]. Once in the ground segment, the data are azimuth compressed (and range compressed if necessary) to produce two-dimensional images with a spatial resolution of 26 metres in range and between 6 and 30 metres along track, depending on the number of looks used.

The ERS-1 mission, like SEASAT, is oriented primarily towards ocean and ice monitoring and its main objectives are to develop and promote applications related to a better knowledge of ocean parameters, sea state and ice conditions and to increase the scientific understanding of coastal zones and ocean processes. To this end, it is expected to have a lifetime of not less than two years and will be followed by ERS-2 in 1994. As far as the SAR is concerned, this instrument and mission will be identical to ERS-1, it will simply provide continuity of data gathering. Although in many ways a satellite conceived in the image of SEASAT, results from ERS-1 will provide an invaluable comparision with SEASAT data as both its frequency band and polarization are different.

In complete contrast, although the Soviet space agency, Glavkosmos, has also been active in the development of spaceborne SAR, it is with an instrument significantly different from its Western counterparts. The operational satellite is known as ALMAZ (diamond) and the first in the series was launched on 31 March 1991 from Baikonur Cosmodrome. It was preceeded by a prototype system, the enigmatic platform, COSMOS-1870. COSMOS-1870 was built and prepared for launch in 1981, so was very much of the SEASAT generation. However, the launch was cancelled and all further work on the project was suspended. The satellite was, however, saved from destruction and eventually launched into orbit on a PROTON booster from the Baikonur Cosmodrome launch site on 25 July 1987 [11]. It appears that the ALMAZ satellite system will have both civil and military applications, totally unlike the two Western systems described [12,13]. The principal parameters of the ALMAZ SAR are given in table 3, below.

Frequency	3 GHz
Wavelength	10 cm
Pulse length	0.07 μs
Bandwidth	n/a
PRF	3000 Hz
Polarization	HH
Swath width	2 x 40 km (instantaneous) 2 x 350 km (maximum)*
Incidence angle	30-60°
Resolution	15-30 m
Looks	4**

Table 3 : ALMAZ SAR Parameters

* Achieved by physically rolling the spacecraft
** Assumed, from 15 metre antenna length and 30 metre resolution

The radar carried on COSMOS-1870 and its ALMAZ successors is significantly different from other spaceborne SARs to warrant some discussion. The principal difference is that the radar does not use pulse compression to achieve high range resolution. Rather, it uses a short duration, high power, constant frequency pulse. This has major implications on the design of the spacecraft. It requires more prime power for the radar, and hence it has larger solar panels (some 86 square metres in area, supplying 2.5 kW). This, in turn, means greater atmospheric drag at its orbital altitude of 265 km, requiring frequent manoeuvres to prolong platform lifetime. Consequently, the spacecraft itself, figures 11 and 12, had an in-orbit mass of 18.5 tonnes of which only 4 tonnes were payload (cf. a mass of 2.3 tonnes for ERS-1 and a payload of 1000 kg) to provide sufficient fuel for the required manoeuvres over the satellite's two year design lifetime. From published photographs, the spacecraft appears to be based on a SALYUT space station module, although it is, of course, unmanned. The design vintage also has implications on the design of the SAR. As the Soviets were behind in coherent transmitter technology at the time it was designed, the SAR was conceived as a phase locked magnetron based design. In this design, the frequency stability requirements of the prime R.F. power source, the magnetron, can be relaxed, with the required phase coherence being supplied by a highly stable crystal oscillator. Return signals are down-converted and stored on an analogue magnetic tape recorder of 6 MHz bandwidth. A limited linearity, rapid reacting AGC system is used in the receiver to compress the dynamic range of the signals. The requirement for this process is a consequence of the ground station optical processor, which itself has a limited dynamic range. At an appropriate time, data are down linked over an analogue data link for processing [14]. Another significant difference between ALMAZ and other spaceborne SARs is that it is equipped with two antennas enabling imaging on either side of the ground track, although not simultaneously. The radar antennas are of slotted waveguide design, with an overall size of 15 metres by 1.5 metres. They are divided into three hinged panels for launch requirements. In terms of radar parameters, ALMAZ appears to be virtually identical to COSMOS-1870, the only real differences being wider swaths and slightly higher resolution.

Other differences between ALMAZ and its predecessor are in data handling. The data is to be processed digitally rather than optically as it was for COSMOS-1870, the satellite will be used in conjunction with geo-stationary data relay satellites for near real-time operation, and its data down link will be digital rather than analogue as it was for COSMOS-1870.

Maritime applications of ALMAZ are broadly as for other SARs, but it appears that monitoring the ocean is not its primary function. Specific objectives to be studied will be the distribution and dynamics of currents, the spatial structure of wave formations, the evaluation of surface winds, the topography of the ocean floor, the identification of oil spills, the state of ice cover and its seasonal fluctuations and the identification of navigational hazards [15].

4. MARITIME APPLICATIONS OF SAR

The preceeding sections illustrate that spaceborne SAR is potentially a very effective sensor in the maritime environment, and that a wide variety of phenomena may be imaged in this particular application. Several of the more important of these phenomena will now be discussed in more detail.

To fully understand and characterise the nature of SAR images of the ocean surface, it would be necessary to understand the interaction between the electromagnetic radiation and a portion of the ocean surface which has a dimension of some tens of metres. This interaction is a highly complex process since, on this given scale, the ocean surface is constantly changing as a result of processes such as capillary waves, gravity waves, swell and orbital motion. Nevertheless, it is possible to produce a reasonable, if not fully comprehensive, description of the type of features which are likely to be observable in SAR images of the ocean surface.

The first and, perhaps, most obvious phenomenon seen in SAR images of the ocean surface are surface waves, since they are the most common feature found on the oceans. Surface waves with a wavelength similar to that of the radar will return an enhanced backscatter signal due to Bragg scattering [16]. For an L-band radar, such as SEASAT, short gravity and capillary waves dominate the backscattered signal. Any modulation which disturbs the small scale surface wave pattern will be detectable in the radar image. Such modulations include; land, man-made objects, waves, currents and oil slicks. An example of SAR response to surface waves is shown in figure 13. This shows a SEASAT image of the sea around the island of Foula off the Western coast of Mainland, Shetland. In this image, which is oriented approximately north-south, the along track direction is vertical and the range direction, horizontal. The surface waves are visible in the radar image as a periodic regular change in the image tone, that is, alternating bright and dark streaks which are extended predominantly in the along track direction. This image is complicated by the presence of Foula itself which causes the ocean waves to be refracted and subsequently to interfere causing complex modulations. The whole SEASAT image, from which this is an extract, was acquired in fourteen seconds, and thus represents an almost instantaneous "snapshot" of the wave pattern over the region. In the open ocean, such modulation effects as seen in the Foula image will be minimal and the predominant feature will be the bright and dark streaks. These streaks are caused by the shape of the waves themselves. The front of the wave will be at an angle which reflects much of the incident electromagnetic radiation back to the radar, whereas the back of the wave will be at an angle which causes very little reflection. Consequently, the SAR's response to surface waves will be largely dependent on the imaging geometry with respect to the direction of propagation of the waves. Most often, waves propagating in the range direction are imaged, as might be expected, but along track travelling waves are also seen in SAR images from time to time [17].

The imaging of ocean waves is important in several specific applications. Surface waves are generated by the wind. Therefore, the characteristics of the surface waves is an indirect measure of the wind characteristics. This, obviously, has considerable application in weather forecasting. A major limitation of present day forecasting is a lack of data over open ocean areas. Whilst this is a particularly severe problem in the vast oceanic areas of the Southern hemisphere, it is also of great importance in the Northern hemisphere, due to the reducing number of weather ships in the Atlantic Ocean [8]. The series of spaceborne SARs planned for the next decade, in particular the European Space Agency's ERS and POEM (Polar-Orbit Earth-observation Mission) programmes, will provide a new and regular source of data, which will be of great benefit in

medium range weather forecasting for Europe. The other major application of SAR ocean surface wave imagery uses the wave information directly. The information used is in the form of ocean wave spectra produced by carrying out a Fast Fourier Transform (FFT) on the original SAR image. These wave spectra are a measure of the energy in the waves as a function of propagation direction and wavelength [18]. In particular, the direction and wavelength of swell wave systems can be measured readily from the spectra and a series of such spectra can be used to determine the evolution of the swell wave systems [19]. Such information is of great importance for low-lying coastal areas, which can suffer major disasters caused by wave action.

In certain shallow ocean areas imaged by SAR, surface phenomena are detected, often in great detail, that appear to be induced by the local bathymetry, or sea bottom relief. The most striking examples occur in images of shallow water areas, where strong currents flow over uneven bathymetry. These images show pronounced surface expressions closely delineating the bottom features. In other areas, particularly near islands and coral reefs, more subtle changes in surface expression that reflect the bathymetry have been imaged. The mechanism by which the sea bottom relief affects the ocean surface, and thereby the radar backscatter, are largely unknown. However, likely theories have been put forward [4,7]. This capability to image the sea bottom relief by its manifestation on the surface has great application in the identification of potential navigational hazards to shipping, and in ship routing. Figure 14 shows a COSMOS-1870 image of the Iranian port of Bushire in the Persian Gulf. Sea bottom relief can be seen below and to the left of the peninsula, and in particular the dredged channel for ship traffic and its associated navigational buoys [20].

The high resolution of SAR reveals ships and their associated wakes in a large proportion of ocean imagery. Both stationary and moving ships appear typically as bright point targets against a speckled sea background, with moving ships accompanied by one or more wake features, figure 15. Detection of a ship by SAR depends on several factors. Firstly, the size, shape, and structure of the ship itself are important, as is its orientation to the radar beam. It also depends on the general sea state and the wind velocity; high winds and waves tend to mask the ship's image. The inherent speckle in the SAR image will also be a contributory factor to this masking effect. However, this application is potentially very important, in both the civil and military domains. The frequent opportunities for wide area surveillance from a spaceborne instrument, particularly in Northern latitudes, coupled with the all-weather, day and night capability of SAR offer an ideal means of monitoring large maritime economic zones [21,22], and the military use of spaceborne radar for ocean surveillance is far from a new idea [23]. In addition, the high resolution of SAR and the mechanism of the interaction between electromagnetic radiation and the sea surface give a spaceborne SAR several more advantages, than just all weather, day and night operation, over other potential surveillance sensors. The potential to detect ship parameters, other than simply its presence at a particular location, is possible. These parameters include; size, speed, direction of motion hull characteristics and superstructure and their determination will be described below.

In general, it is the ship itself and its intensity distribution or its effect on the sea surface around it, that is its wake, that determine these parameters. Those parameters dependent on the various wake components that might be imaged are considered first. Several distinct wake features are seen in SAR imagery, figure 16. These include; bright vee-shaped wakes, dark vee-shaped wakes, dark linear wakes, single arms of vee-wakes and the waves associated with ship wakes. These different wake components are generated by different mechanisms, as summarised in figure 17. Potentially, these wake features offer a great deal of information, beyond simply the presence of the ship that caused them.

A moving ship produces surface irregularities over a wide range of frequencies. The main energy, however, usually goes into two ship generated surface wave components. These are the bow waves and the stern waves (diverging and transverse wave crests), as shown in figure 18. The whole wave pattern is called the Kelvin wake, after Lord Kelvin, who determined the mathematical solution in 1887 [24]. A geometric line drawn through the points where the bow, or cusp, and stern wave crests disappear, mark the edge of the Kelvin wake. These lines form an angle of 19.5 with the ship velocity vector and are usually called the Kelvin arms or the Kelvin wake envelope. A typical Kelvin wake, imaged by a SAR is shown in figure 19. The two Kelvin arms can be seen either side of the horizontal dark turbulent wake, offset from the image of the ship itself. The reason for this displacement of the ship from its associated wake features will be fully explained later. This ship and wake pair is, in fact, that near the right hand edge, below

centre of figure 15. The imaging mechanisms causing the Kelvin arm imaging are very complicated. The simplest model is that the imaging is caused by tilt and hydrodynamical modulation of Bragg waves, which in turn causes radar backscatter modulation. Most ships in motion will produce a Kelvin wake, but the relative amount of energy fed into it will depend on the ship itself and its motion.

Narrow vee wakes are also features of ship generated surface waves. These are caused by waves of Bragg resonant wavelength, radiating away from the ship track. The opening half-angle of the narrow vee wake is given by :

$$\tan\alpha = (\lambda g/4\pi\sin\theta)^{1/2} \sin\varphi/2V_{ship}$$

where; λ is the radar wavelength, θ the angle of incidence and φ is the radar look direction with respect to the ship track. Consequently, the opening angle is largest for azimuthal, or along track, ship motion and collapses to zero for range motion, creating a "bright turbulent wake". In contrast to the Kelvin wake components, the narrow vee wake is not imaged through modulation of the existing surface Bragg waves, but through direct observations of the Bragg waves produced by the ship. Typical narrow vee wakes can be seen in figures 5 and 16, where both bright and dark vee wake features can be seen. In some cases, only one arm of the vee wake is imaged.

The most frequently observed ship wake phenomenon in SAR imagery, is a dark linear feature, behind the ship, extending for perhaps several kilometres. This feature is usually called the turbulent wake. It is caused by the turbulence, in the stern wake, of the passage of the ship through the water temporarily damping out any capillary waves and small surface gravity waves which results in a lower radar backscatter than the surrounding sea surface. Typical turbulent wakes can be seen in figure 15, and the expanded portion of this image in figure 19.

The final wake effect is caused by ship generated internal waves. These are generally believed to be produced by hull vortices in the presence of a highly stratified water column, as shown in figure 20. These are very seldom seen in spaceborne SAR imagery, and the information deducible from them is limited as the stratification of the water column is required, as is an adequate model for hull generated vortices.

A study carried out by the Norwegian Defence Research Establishment (NDRE), on behalf of ESA, has analysed over 200 SEASAT ship wake images, to determine the characteristics and problems associated with SAR detection of ships and ship wakes [21, 22, 25]. One objective of this study was to determine the frequency with which the various ship wake phenomena are imaged. The results of this investigation are presented in table 4, below.

Wake Type	Occurrence
Dark turbulent wake	85%
Kelvin arm(s)	35%
Narrow vee-wake	5%
Stern waves	1%
Others	7%

Table 4 : Occurrence of Various Ship Wake Components

Clearly, the dominent wake feature is the dark, turbulent wake. Assuming a typical ship speed of 8 ms^{-1} ($\approx$15.5 knots), turbulent wakes were found to persist for some seven minutes. The visibility of the different wake components is highly dependent on environmental conditions, radar wavelength, resolution and look angle. Consequently, different SARs will have different capabilities in imaging wake components. A discussion of this phenomenon, with respect to SEASAT and ERS-1 will follow later.

In summary then, there are four principal wake components that may be imaged by the SAR :

i) The narrow vee-wake - A ship-generated surface wave resulting from a Bragg scattering mechanism.

ii) The Kelvin wake - A ship-generated surface wave generated by the longer gravity waves.

iii) The turbulent (or vortex) wake - resulting from the damping of capillary waves and small surface gravity waves by turbulence.

iv) Ship-generated internal waves - produced by the presence of a strong, shallow density gradient.

The application of the presence of one or more of these wake phenomena in SAR imagery will now be discussed. The most obvious information that can be derived from the image of a ship's wake is the course of the ship. This is most applicable to the dark, turbulent wake, since both arms of a vee-wake may not be imaged and consequently an incorrect interpretation of the ship's course could be made. An ideal example of the potential to determine a ship's course from the imagery of its wake is figure 19. Here, both the dark turbulent wake and the Kelvin wake have been imaged, giving a high level of confidence for the ship's estimated course.

The second useful piece of information that can be obtained from wake imagery is the speed of the ship. This may be determined in several ways, depending on the particular wake component(s) imaged. For a narrow vee-wake, the opening half-angle is indirectly proportional to the ship's speed, V_{ship}. Thus, by measuring the opening angle, it is possible to make an estimate of the ship's speed. If the transverse stern waves in the Kelvin wake envelope are imaged, as they are in figure 19, then the ship's speed can be estimated by the relationship $\lambda_s = 2\pi V_{ship}^2/g$, where λ_s is the wavelength of the stern waves. A further method of determining the speed of a ship through the SAR image of its wake is also evident in figure 19. It will be noted that the ship itself, in this image, is displaced from the wake components. This is a direct consequence of the SAR imaging mechanism. The SAR assumes that targets are stationary and that the Doppler shift of the received signal is due entirely to the radar motion. However, ships are usually in motion, and it is this that has an influence on the image. The ship is in motion, whereas the sea surface is, to all intents and purposes, stationary. Consequently, the radar interprets the different Doppler shifts of the ship and the sea surface as different azimuth locations. So, the primary influence of target motion on the SAR image is a displacement of the target from its true position in the image to a new position, appropriate to its velocity, provided that the velocity is not greater than the apparent velocity of stationary targets at the edge of the antenna beam. If the velocity is too large, the target will not be imaged at all. Targets moving towards the radar are displaced in the direction towards which the radar is moving, and those moving away are displaced in the opposite direction, figure 21. The displacement, x, as a function of the radial component of target velocity, v_t, is calculated using the following relationship between position and Doppler shift, Ω :

$$x = \lambda r\Omega/2v$$

and the expression for the Doppler shift of a wave reflected from a moving target :

$$\Omega = 2v_t/\lambda$$

to obtain the apparent displacement of the target in the image :

$$x = v_t r/v$$

Using SEASAT values of $r = 850$ km and $v = 7.5$ kms^{-1}, a target moving at 1 ms^{-1} towards the radar is displaced 113 m in the azimuth (along track) direction in the image [26].

Both the displacement method and measurement of the wavelength of the stern wave spectrum have been carried out for the ship in figure 19. Both techniques give a result for the ship's speed of 12 ms^{-1} (23.3 knots). So, two independent methods give the same result, leading to a high level of confidence for ship speed measurement from wake imagery. The dark turbulent wake is less useful in determining a ship's speed, unless there is azimuthal Doppler displacement of the ship.

Subjectively, it may be possible to estimate hull characteristics from ship wake imagery. Measurement of the length, width and backscatter modulations of the turbulent wake could provide hull information, providing sufficient environmental data and an adequate imaging model were available. The stern wave component of the Kelvin wake envelope could be used for a rough first approximation at ship classification. In general, merchant vessels would be expected to travel at economic speeds. Consequently, their stern waves will be of low amplitude. Military vessels, on the other hand, operate at any speed and can thus produce stern waves of significant amplitude. Another possible use of the Kelvin wake envelope has application for ships such as oil tankers. Empty ships, riding high in the sea, will produce breaking waves, much foam and only weak Kelvin arms. A heavily loaded ship riding low in the sea, on the other hand, will, at the same speed, produce little foam and a strong Kelvin wake.

As noted above, the visibility of the different wake components is dependent on several factors, some of which are directly related to the SAR itself. A comparison between the expected results from ERS-1 and the archive data from SEASAT has been carried out [22] with regard to this phenomenon. ERS-1 is expected to be somewhat better than SEASAT at imaging stern waves because of the greater modulation of the shorter wavelength Bragg waves, particularly in the case of low wind speeds. Similarly, ERS-1 is expected to be better than SEASAT at imaging the Kelvin arms. However, preliminary results indicate that the ERS-1 C-band SAR will have serious trouble detecting turbulent wakes, particularly at wind speeds of higher than 5 ms^{-1}. It seems clear that an L-band SAR, such as SEASAT's is to be preferred for the detection of dark turbulent wakes, because only the surface modulations giving enhanced returns of L-band wavelengths will survive moderate to high wind speeds. This comparison of observability between different radar bands will be an interesting aspect of ERS-1 operations.

So much for information potentially gleaned from a ship's wake. What of the ship itself? At the resolution of the SARs discussed, large vessels, at least, should be resolvable into major scattering centres, potentially indicating details the ship's structure leading to the possibility of classification. Figure 22 shows the ship from figure 19 in more detail. Here, the ship has been expanded, density sliced and in figure 22a, false colour has been applied to the intensity scale. Some structure is evident. In figure 22b, further enhancement, in terms of a z-modulation, has been applied, giving a 3-dimensional effect to the ship's image. The ship in question in this image was a bulk carrier, of which the image could be taken to be a reasonably realistic representation. Similarly, figures 23 and 24 show similar effects for another vessel, this time believed to be a military vessel. The expanded ship of figure 24 is the central vessel of the main ship group in figure 23. In figure 24, a different image processing technique has been used with the same result; a pseudo 3-dimensional representation of the ship. In this image, the ship's structure is significantly different from figure 22b, with the main scattering centres clustered towards the centre of the ship, rather than at the extremities. Since, in general, military vessels can have very distinctive outlines, this technique may be useful in distinguishing between commercial and military vessels [22,23].

In recent years, considerable effort has been put into the automatic detection of ships in SAR imagery. This is particularly true of Europe, as a consequence of the forthcoming launch of ERS-1. In particular, both the U.K. Defence Research Agency, Aerospace Division, Farnborough [27] and the Norwegian Defence Research Establishment, Kjeller [28] have been active in the field. The schemes proposed by both are essentially the same, only the particular algorithms employed in the processing differ. The overall concept is firstly to detect possible ships as bright point targets, and then to confirm positive ship detection by the presence of wake features. It is in this second stage that the techniques employed by the two countries differ.

The Norwegian approach is to first look for ship targets and subsequently, to look, in a circle, around the location of candidate ship detections for a characteristic wake signature in a scan of radar backscatter. The philosophy behind this scheme is that the ship is a more robust target under varying wind, wave and aspect angle conditions.

The approach adopted by the U.K. is to detect wakes as linear features in the image and correlate them with location of possible ship detections. The main wake detection technique uses the Hough transform to detect linear features. The Hough transform is a special case of the Radon transform, which although not as fast, is conceptually simpler and is readily analysed [29]. The Hough transform parameterises all possible lines in an image in terms of quantised r, distance

from the centre of the image, and θ, the angle it makes with the y-axis, values, figure 25. Each (r,θ) point is assigned the mean intensity of pixels lying along its corresponding line. Bright and dark lines in the image, therefore, transform to local maxima and minima in the (r,θ) space [30]. A typical Hough transform of a ship wake image is shown in figure 26. The various wake components, having different positions and orientations cause peaks at different positions in the Hough transform. The vertical axis of the Hough transform indicates the orientation of the wake component in the image and the horizontal axis represents its distance from the centre of the image. A second algorithm is then used to locate the end points of each line detected. The output from this stage is a set of fragments defined by the x,y co-ordinates of the two ends. A subsequent algorithm removes multiple detections and links fragments to span gaps in the lines detected. A final algorithm associates the lines with ship locations, using the knowledge that a ship will be at the same range as the vertex of its wake, but may be shifted in azimuth. The results of these algorithms on a SAR image is shown in figure 27. Detail from a SEASAT image of a fishing fleet off Ballyquintin Point is shown, together with an image of the wake skeletons detected in the image using the procedure described above. In this case, the wakes in the original image were bright features and detection, as such, was not necessary. However, the technique is particularly useful when the wakes are weak features embedded in a sea background of varying intensity.

The U.K. approach to ship/wake detection has been applied to the development of a ship detection workstation (SDWS), which will be capable of obtaining results in the form of operationally useful shipping reports for a single 100 km x 100 km ERS-1 SAR scene in under three hours from the satellite overpass [27,31].

So, potentially it may be possible to determine; the presence of a ship, its course, speed and make an estimate of its classification from a sensor capable of all weather, day and night operation at a range of perhaps many hundreds of kilometres. This has tremendous application for both the civil and military domains. However, all this is only true if the signal to noise ratio is sufficient for successful imaging. If a high level of background noise, from whatever source, causes degradation of the SAR imagery to such an extent that ship targets of sufficient radar cross section for normally successful imaging can no longer be identified, the potential capability of the SAR is nullified [32,33].

A final application for spaceborne SAR imagery is that of maritime pollution monitoring. In the same way as turbulence, pollutants, particularly oil, on the sea surface can also damp the capillary waves and small surface gravity waves and so cause a dark feature in a SAR image. Two examples, at least, have been reported. A very long, 30 km, dark, stern wake-like feature imaged by SEASAT on 9 September 1978, is believed to be oil, or an oil contaminated liquid discharged from an associated ship heading towards Delaware Bay [4]. The second example is of an incident during the "Tanker War" in the Gulf, imaged by COSMOS-1870. An extensive oil slick is evident emanating from a tanker believed to have been damaged by hostile action [20]. Thus, spaceborne SAR could be an important tool in monitoring the extent and movement of major oil spills, such as in the Gulf conflict of early 1991.

SAR, thus has many varied applications in the maritime environment in both the civil and military sectors, and it is most likely that its use will grow in this area in the coming decades.

5. THE REQUIREMENT FOR ADEQUATE CALIBRATION

The basic measurement made by a SAR is of the engineering quantity of radar backscattering from the earth's surface. It is from this *engineering* quantity that *geophysical* data products, such as wind fields over the ocean or ocean wave spectra, are derived. Consequently, if quantitative information is to be extracted from SAR images, and if these data products are to be reliable, an adequate level of accurate calibration and validation of the SAR instrument will be required.

Two types of calibration are possible, corresponding to the two quantities referred to above, and they are carried out in two distinct phases. Firstly, engineering calibration, which is defined as the process of converting spacecraft payload telemetry into engineering units within known limits of accuracy and precision. In the case of SAR this is the radar backscattering

coefficient, σ (m^2/m^2). The second step is geophysical calibration, which is the process of converting the engineering quantities (radar backscattering) into geophysical units (winds and waves), within known limits of accuracy and precision [34]. This latter conversion takes place in the processors associated with the spacecraft ground segment and uses models to relate the engineering quantities to the geophysical quantities of interest, and as it does not concern measurement of actual radar parameters, it is not considered further.

The basic engineering measurement made by a SAR is that of radar backscattering coefficient, σ (m^2/m^2). To achieve engineering calibration, SAR ground processors use pre-launch information about the instrument, such as its electronic gain and antenna patterns, orbital information and in-flight measurements of, for example, instrument noise. Variations in electronic gain are corrected for by adjusting the processor gain according to the in-flight response from an internal calibration unit. Antenna gain corrections are derived from transponder overflights. Calibration transponders receive radar pulses from the SAR and retransmit them at known, pre-determined power levels. Any gain variation can then be compensated for in the processor. For reliable calibration, these transponder overflights should be repeated frequently, particular during the SAR commissioning phase of a mission. Similarly, passive calibration can be carried out with arrays of tri-hedral corner reflectors of known radar cross section [35]. Figure 28 shows a SEASAT image of such an array of corner reflectors at Goldstone, Ca. and figure 29 shows a SIR-B image of arrays of both calibration corner reflectors and transponders at sites at Luffenham, Leicestershire and the surrounding area.

6. FUTURE DEVELOPMENTS

The spaceborne SARs so far deployed, and considered in the dissertation, are are fairly conventional in design. There have been no significant developments in system design since SEASAT; indeed, in some ways, SEASAT could be considered to be a more advanced design since it employed a corporate-fed microstrip planar array antenna with a solid state transmitter, whereas ERS-1 and ALMAZ both use slotted waveguide antennas, fed from vacuum tube based transmitters. However, during the decade of the nineteen-nineties, several spaceborne SAR missions are anticipated, some of which, at least, will employ advanced techniques. Future spaceborne SAR systems will use electronically steered (phased array) antennas which will incorporate distributed transmit/receive modules [36]. Such a distributed SAR system is shown in figure 30. The transmit/receive modules will each contain a solid state power amplifier, switches and phase shifters, as shown in figure 31. The advantage of this technology will be a reduced risk of catastrophic failure and greatly increased flexibility in design and operation.

A typical proposed system design for a SAR of the type described above is the instrument proposed for deployment on the first ESA polar platform mission (POEM-1) scheduled for launch in 1997. SAR is considered to be a core instrument for this mission and its successors. The concept for this SAR is referred to as V-SAR (Versatile SAR) and has been developed in the U.K. [35,37,38,39]. The key concept of VSAR is that it will employ active phased array technology. VSAR will have a 10 metre by 1.3 metre active antenna with five mechanical panels. Each panel will support 4 "tiles" or sub-panels. Each tile will be a seperate component of the active antenna with each tile consisting of a front-fed microstrip patch radiating panel, 0.64 metres by 0.96 metres in size, fed by 16 transmit/receive modules. In addition to the active antenna, the VSAR instrument will also consist of a central unit mounted on the spacecraft and containing the common RF amplifiers and the data handling and control system. The RF signal distribution between the tiles will be via waveguide. The instrument concept of VSAR is shown in figure 32. VSAR will also operate in a multi-mode manner. It will employ conventional beam steering, through the use of the phased array antenna, in a high resolution, narrow swath mode or employ the technique of ScanSAR to achieve wide swath coverage. ScanSAR achieves wide swath coverage by sequentially imaging a series of different sub-swaths. The critical requirement is that each sub-swath is imaged so as to provide continuous along track coverage. This is achieved by imaging for only part of the maximum synthetic aperture, before switching to another sub-swath. Hence, there is a fundamental trade-off between the number of sub-swaths (i.e. coverage) and azimuth resolution [40]. The ScanSAR technique also requires beam steering in elevation, which is again compatible with the phased array antenna concept of VSAR.

As noted above, the major disadvantage of ScanSAR is that wide swath coverage is

achieved at the expense of a degradation in azimuth resolution. The achievable resolution with a ScanSAR system is typically of the order of tens of metres. Whilst this may be adequate for detection of larger ships, say, it may not be good enough for ship classification applications. One solution that has been proposed to overcome this limitation is the implementation of a multiple phase centre antenna system [41]. This transmits pulses into a single beam and receives the pulse returns on two or more beams, which are displaced in the along track direction. The receive beams are assumed to be coincident in the far field region, differing only in their relative phase centre positions at the antenna. This concept is shown in figure 33. The motivation for this approach is that two or more independent sets of target returns are obtained if the distance between phase centres is suitably set. The operating PRF can therefore be reduced compared with a conventional system for a given spatial resolution, as the total number of independent samples for a given target is maintained by the use of the multiple received beams. Preliminary consideration of system performance has concluded that a three receive beam system could provide approximately 120 km continuous swath coverage at a spatial resolution of 3 metres [42].

However, such systems are very much concepts for the future. More immediately, the Canadian RADARSAT, figure 34, is scheduled for launch in 1994. This system will incorporate some of the features previously described. The principal parameters of the RADARSAT SAR are given below in table 5.

Frequency	5.3 GHz
Wavelength	5.7 cm
Pulse length	36.4 μs
Bandwidth	11.58 or 17.28 MHz
PRF	1300 - 1375 Hz
Peak power	10 kW
Polarization	VV
Swath width	500 km *
Incidence angle	20° - 45°
Resolution	25 - 30 m
Looks	4

Table 5 : RADARSAT SAR Parameters

* 10 overlapping swaths of 100 km

Most significantly, RADARSAT will employ an electronically steerable antenna. Ten primary beams, each approximately 100 km wide, will be overlapped within an overall swath of 500 km (operational swaths). In addition to these ten primary beams, there will be a further six experimental beams, overlapped across a further 300 km region (exprimental swaths). Beam switching through the maximum variation in incidence angle (35°) will be achieved in less than one second. The maximum radar on time will be 20 minutes in sunlight and 8 minutes in eclipse on each 105 minute orbit of 1007 km altitude. The transmitter will be based on a C-band klystron tube of 10 kW peak power, rather than a solid state amplification scheme.

The beam switching capability of RADARSAT is of particular interest in the maritime environment, as the near beams in the operational swath, with its low incidence angles, can be used for ocean wave measurement and ice type discrimination, while the far beams, either operational or experimental, can be employed in ship detection and ice feature detection of ridges and icebergs [43].

The principal mission motivation for RADARSAT is for sea ice reconnaissance over the primary Artic transportation corridor, the North-West Passage [44]. Image data from the SAR will be relayed via the ANIK communications satellite to an ice information centre where data from other sources will be assimilated to provide a forecast of ice conditions. This information will then be relayed, again via communications satellite, to users in the form of annotated images.

RADARSAT is a good example of the operational use of spaceborne SAR in the maritime environment, and, leaving aside ERS-1, is the first of a number of missions planned for the decade of the nineteen-nineties. A list of the scheduled and proposed missions is given in table 6, below.

SIR-C/X-SAR	USA/Ge/It	1991/2
JERS-1	Japan	1992
RADARSAT	Canada	1994
ERS-2	ESA	1994
Op. ALMAZ	USSR	1993/4
POEM	ESA	1997
EOS	USA	1998

Table 6 : Future Spaceborne SAR Missions

7. CONCLUSIONS

Spaceborne SAR is obviously a potentially powerful sensor in the maritime environment. Its active nature imparts an all weather, 24 hour imaging capability, limited only by orbit and power supply constraints. It is able to image a variety of ocean phenomena, leading to a range of applications in several fields. The potential for spaceborne SAR in this application is reinforced by the number of missions planned for the future. With these projected missions, a new era in ocean monitoring is just beginning. This potential is exemplified by figure 35, the first ERS-1 SAR image to be acquired at the ESA ground station at Fucino (Italy) during the night of 27/28 July 1991. The scene is located in the North-West of the Netherlands, including the region of the Western Frisian Islands and covers an area of approximately 95 x 95 km. Many of the features, both natural and man-made, of interest in the maritime environment which have been described earlier in this dissertation are present in this image.

8. ACKNOWLEDGMENTS

I would like to thank the following; my course supervisor, Dr David Nixon of Portsmouth Polytechnic for his comments and advice in writing this dissertation, Dr Phil Baldwin of the Defence Research Agency Maritime Division for his comments and support, colleages at the Space Department, Defence Research Agency Aerospace Division, Farnborough and the Space and Defence Research Laboratory, GEC-Marconi Research Centre, Great Baddow for allowing me to use the examples of SAR imagery and finally, my wife, Judith, for her patience in proof reading the draft copy.

9. REFERENCES

[1] Wiley C A — Pulsed Doppler Radar Methods and Apparatus. US Patent 3,196,436 filed 13 August 1954, patented 20 July 1965.

[2] Cantafio L J — Space-Based Radar Handbook. Artech House, Norwood, Ma., 1989.

[3] Skolnik M I — Introduction to Radar Systems (Second Edition) McGraw-Hill Kogakusha, Tokyo, 1980.

[4] Fu L-L & Holt B — SEASAT Views Oceans and Sea Ice with Synthetic Aperture Radar. NASA / JPL, Pasadena, Ca., 1982.

[5] Lewis D J & Wilson C — Description of the EODC SAR Processor. Remote Sensing Society Conference, Bristol, 13-15 September 1989.

[6] — Synthetic Aperture Radar (SAR) Processor : Product Description. Marconi Space Systems, Portsmouth, 1990.

[7] Elachi C et al — Spaceborne Synthetic Aperture Imaging Radars : Applications, Techniques and Technology. Proc. IEEE Vol 70, No 10, October 1982.

[8] Vass P & Handoll M — UK ERS-1 Reference Manual. EODC, Farnborough, January 1991.

[9] Vass P et al — ERS-1 : An Introduction. EODC, Farnborough, June 1990.

[10] Francis R et al — The ERS-1 Spacecraft and its Payload. ESA Bulletin No 65, February 1991.

[11] Yefromov G — On the Completion of the Flight of the COSMOS-1870 Satellite. Sotsialisticheskoya Industriya, Moscow, 1 August 1989.

[12] — Soviets Seek French Payload for Use on Large Earth Observation Platforms. Aviation Week & Space Technology, 20 November 1989.

[13] Langereux P — L'URSS Prépare une Série de Satellites-Radar. Air et Cosmos, No 1261, 12 December 1989.

[14] — Radar Sounding of the Earth from the "KOSMOS-1870" Artificial Earth Satellite. Space Commerce Corporation, Houston, Tx., 1989.

[15] — ALMAZ Radar Remote Sensing Satellite Buyer's Guide. Space Commerce Corporation, Houston, Tx., 1990.

[16] Cimino J B & Elachi C — Remote Sensing with Spaceborne Synthetic Aperture Imaging Radars : A Review.

[17]	Keyte G E & Macklin J T	SIR-B Observations of Ocean Waves in the NE Atlantic. IEEE Trans. Geoscience & Remote Sensing Vol GE-24, No 4, July 1986.
[18]		ERS-1 - A Keen Eye on the Earth. ESA Folder F12, August 1988.
[19]		ERS-1 : A Satellite for the 1990s. NRSC, Farnborough.
[20]	Vitter V	Synthetic Aperture Radar Results by KOSMOS-1870. Earth Mission 2000, London, 7 December 1989.
[21]	Wahl T et al	SAR Detection of Ships and Ship Wakes. Proc. SAR Applications Workshop, Frascati Italy, 16-18 September 1986.
[22]	Aksnes K et al	SAR Detection of Ships and Ship Wakes. NDRE, Kjeller Norway, January 1988.
[23]	Dutton Sq Ldr L et al	Military Space. Brassey's, London, 1990.
[24]	Thomson W (Lord Kelvin)	Waves Produced by a Single Impulse. Proc. Royal Society No 42, London, 1887.
[25]		Detection of Ships and Ship Wakes Using SAR Images. ESA Earth Observation Quarterly No 15, September 1986.
[26]	Stewart R H	Methods of Satellite Oceanography. University of California Press, Berkely Ca., 1985.
[27]	Rye A J et al	A Workstation for the Fast Detection of Ships. Proc. IGARSS '90, Washington D.C., 20-24 May 1990.
[28]	Eldhuset K	Automatic Ship and Ship Wake Detection in Spaceborne SAR Images from Coastal Regions. Proc. IGARSS '88, Edinburgh, 13-16 September 1988.
[29]	Quegan S et al	Automatic Interpretation Strategies for Synthetic Aperture Radar Images. Phil. Trans. Royal Society A324, London, 1988.
[30]	Hendry A et al	Automated Linear Feature Detection and its Application to Curve Location in Synthetic Aperture Radar Imagery. Proc. IGARSS '88, Edinburgh, 13-16 September 1988.
[31]	Murphy L M	Use of the Hough/Radon Transform to Detect Ship Wakes in SAR Images. Remote Sensing Society Meeting - Remote Sensing of Ship Wakes, Farnborough, 29 March 1990.
[32]	Condley C J	The Potential Vulnerability to Increased Background Noise of Synthetic Aperture Radar in the Maritime Environment. IEE Colloquium - Synthetic Aperture Radar, London, 29 November 1989.
[33]	Condley C J	Some System Considerations for Electronic Countermeasures to Synthetic Aperture Radar. IEE Colloquium - Electronic Warfare Systems, London, 14 January 1991.

[34]	Attema E & Francis R	ERS-1 Calibration and Validation. ESA Bulletin No 65, February 1991.
[35]		Space Based Synthetic Aperture (SAR) Developments at RAE. Royal Aerospace Establishment at MM(90) folder, Military Microwaves '90, London, 11-13 July 1990.
[36]		The Technology of Future SAR Systems. BNSC data sheet, June 1989.
[37]	Sawyer F G	SAR System Design.
[38]	Sawyer F G et al	The Synthetic Aperture Radar for the European Polar Platform. IEE Colloquium - Synthetic Aperture Radar, London, 29 November 1989.
[39]		VSAR : System Concept Brochure. Marconi Space Systems, Portsmouth, 1990.
[40]	Brown M A & Sawyer F G	Advanced SAR Concepts. Proc. IGARSS '88, Edinburgh, 13-16 September 1988.
[41]	Currie A	Wide Swath SAR Imaging with Multiple Azimuth Beams. IEE Colloquium - Synthetic Aperture Radar, London, 29 November 1989.
[42]	Currie A & Hall C D	A Synthetic Aperture Radar Technique for the Simultaneous Provision of High-Resolution and Wide-Swath Coverage. Proc. Military Micrwaves '90, London, 11-13 July 1990.
[43]	Freeman N G S & McNutt L	Ocean and Ice Measurements from Canada's RADARSAT.
[44]	Raney R K	The Canadian RADARSAT Program.

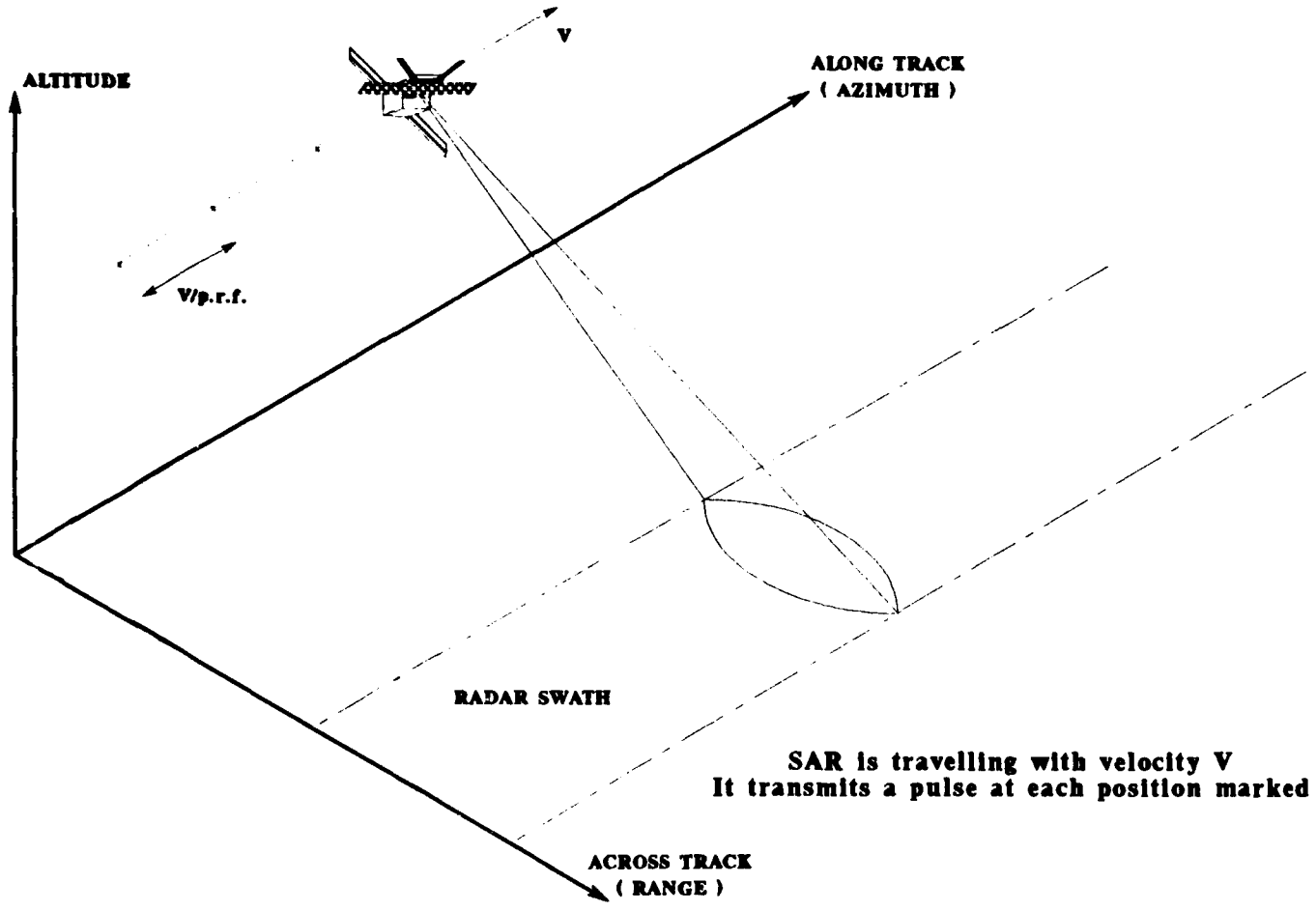

FIGURE 1: Principle of Synthetic Aperture Radar (SAR)

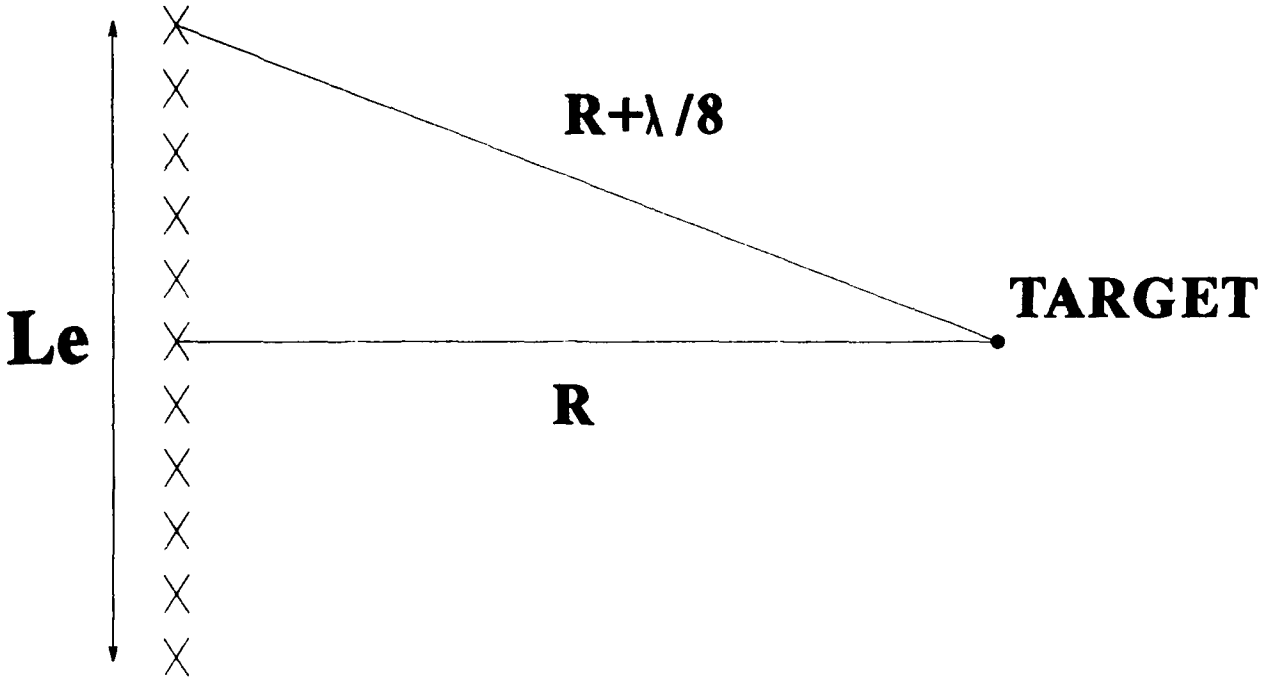

FIGURE 2: Geometry of the Unfocused SAR

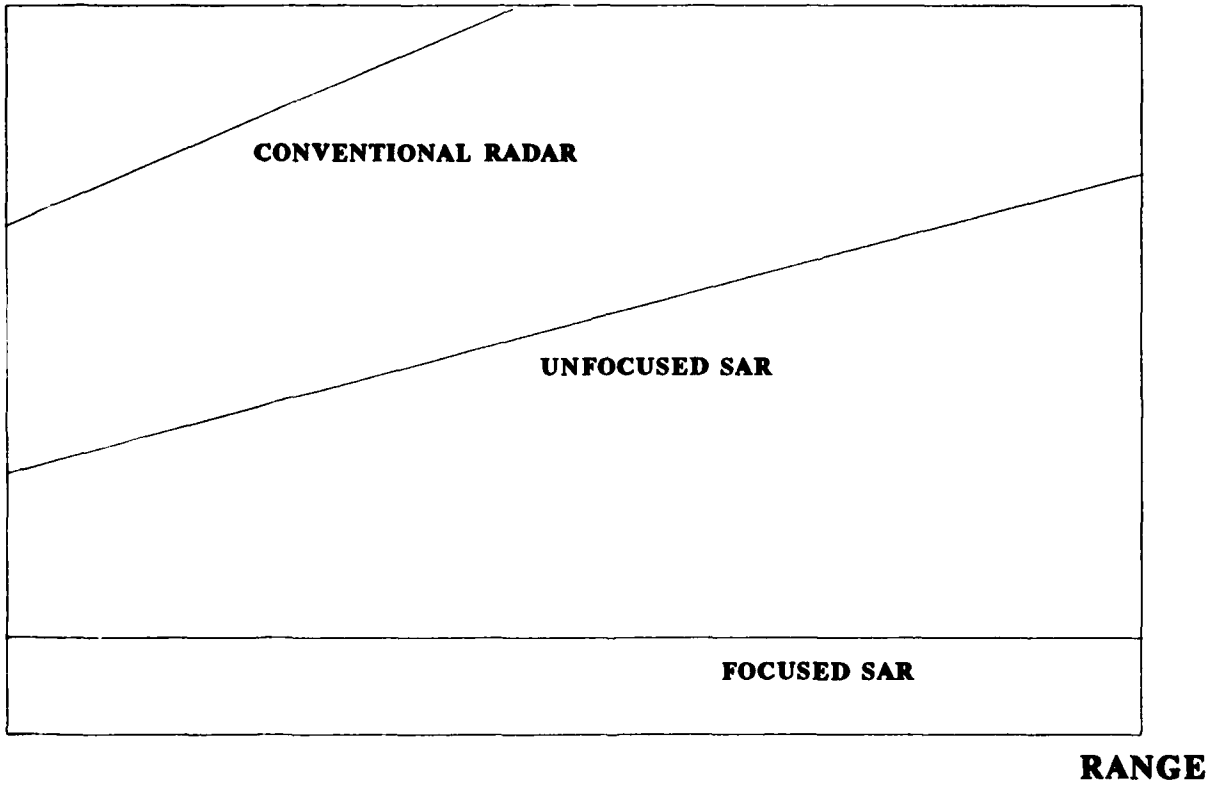

FIGURE 3: Along Track Resolution as a Function of Range

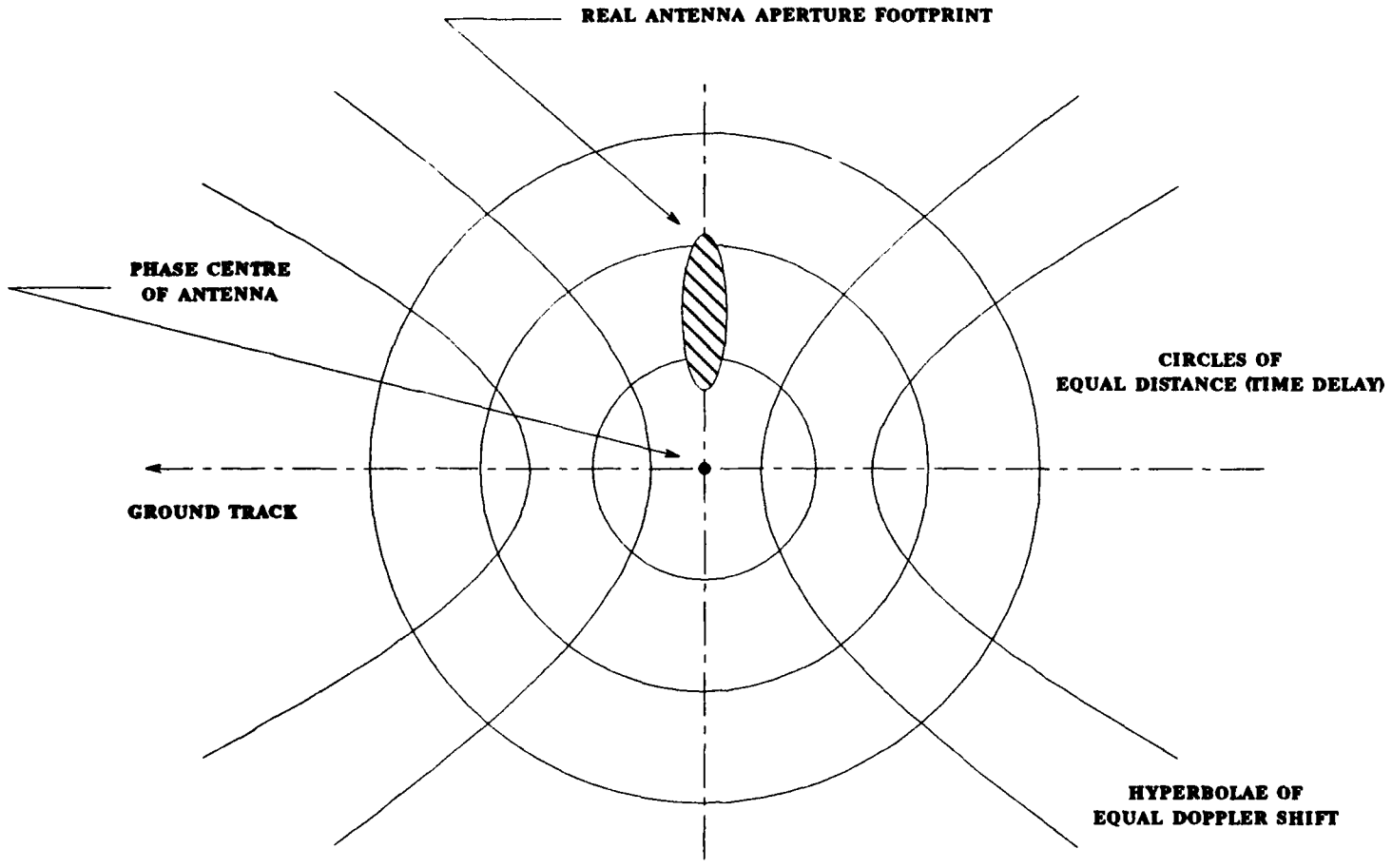

FIGURE 4: Geometry of SAR Illumination on the Ground

Figure 5: SEASAT Image of the Atlantic Ocean off Florida

Figure 6: SEASAT Image of the Solent

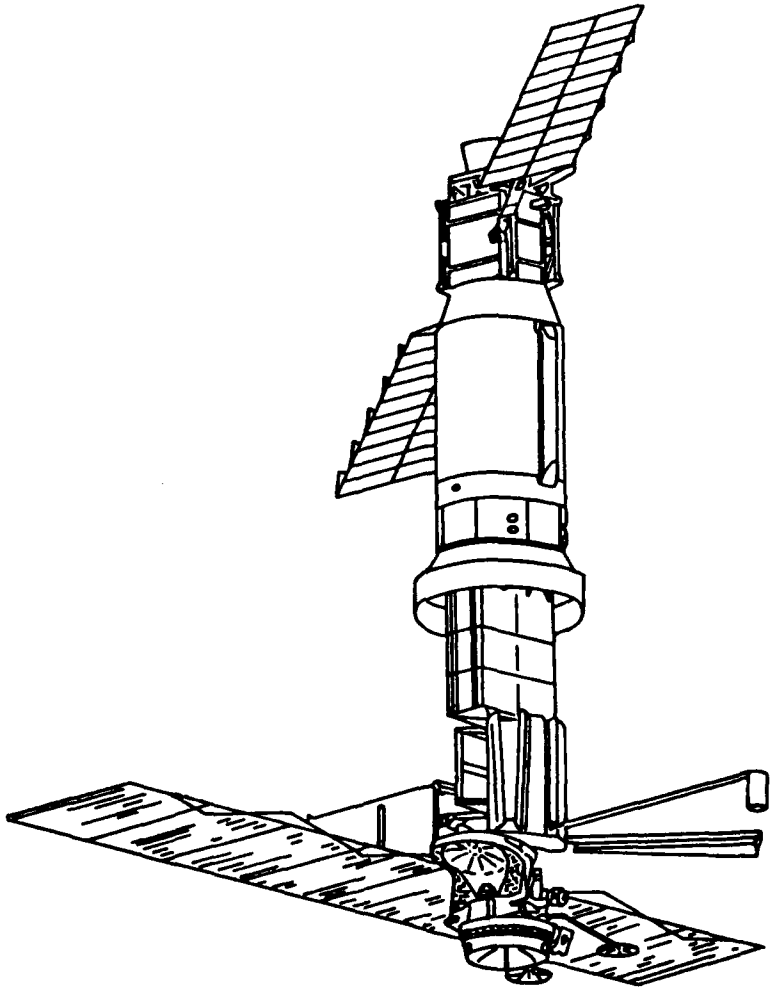

Figure 7: The SEASAT Satellite

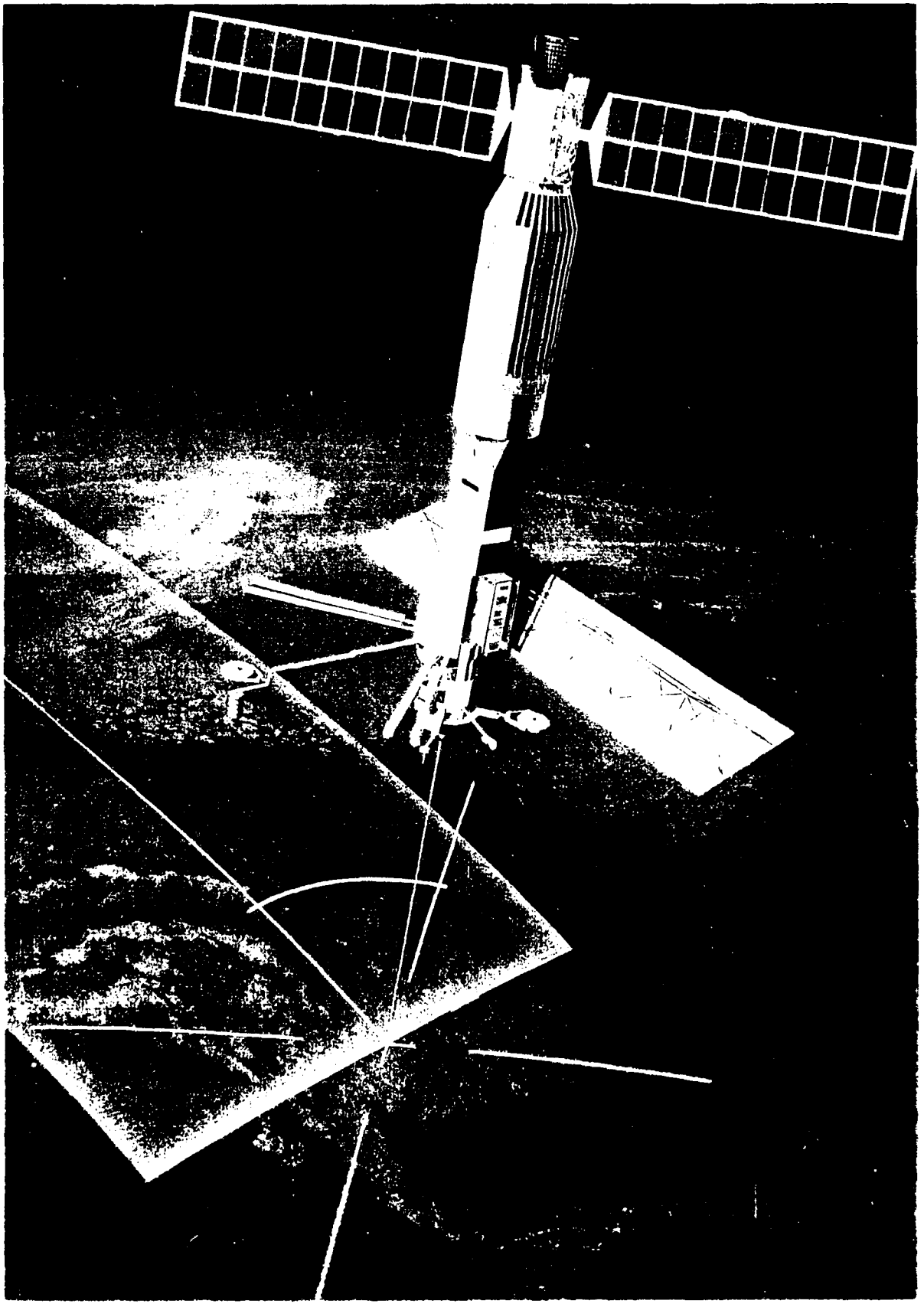

Figure 8 Artist's Impression of SEASAT in Orbit

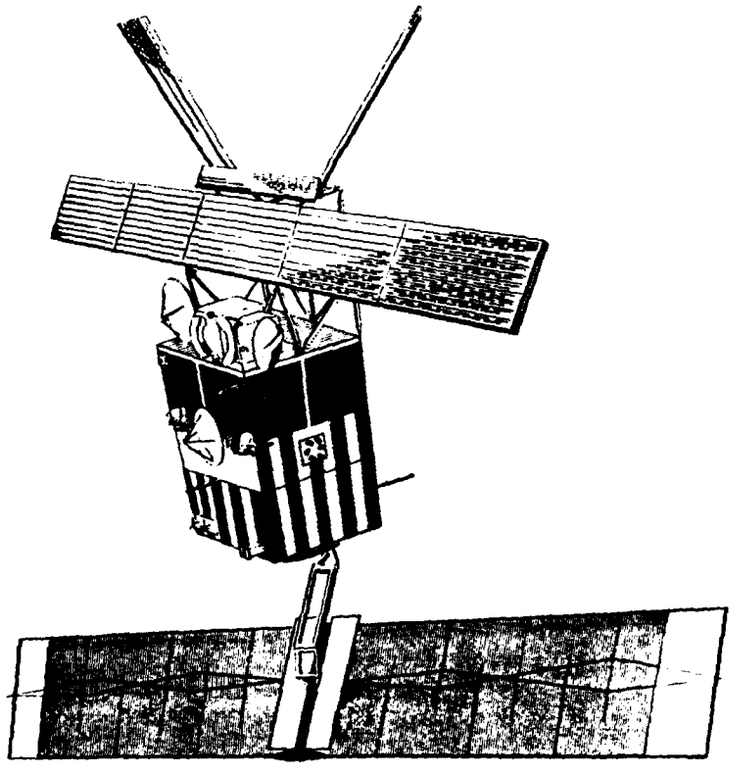

Figure 9: The ERS-1 Satellite

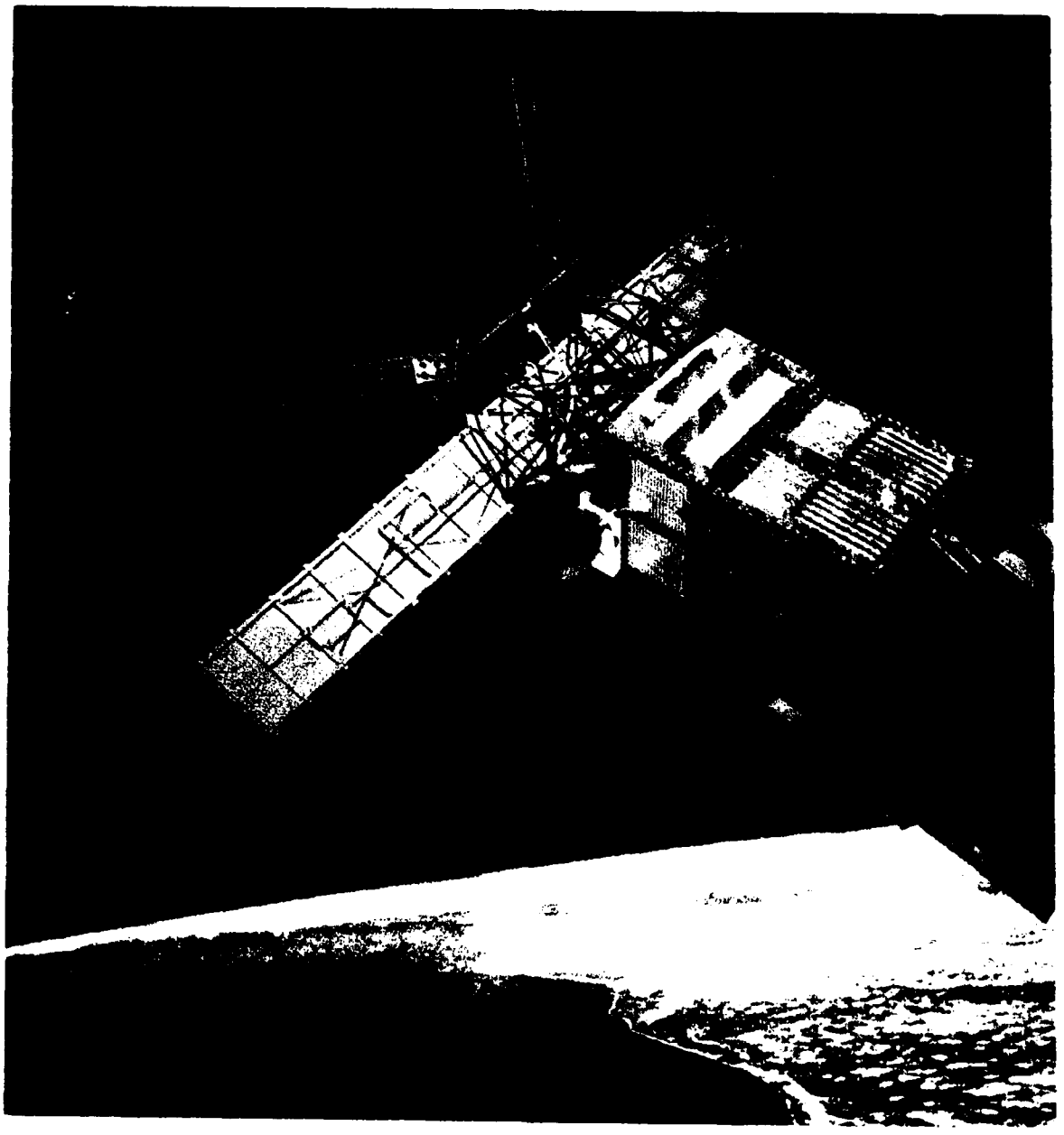

Figure 10: Artist's Impression of ERS-1 in Orbit

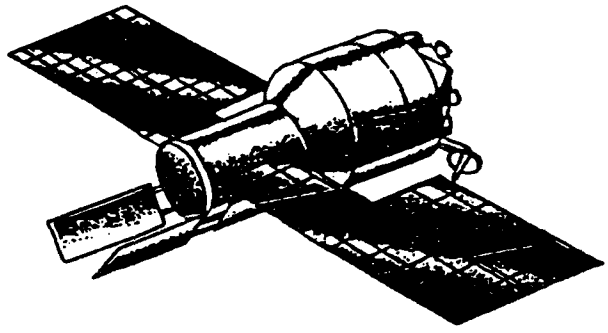

Figure 11: The ALMAZ Satellite

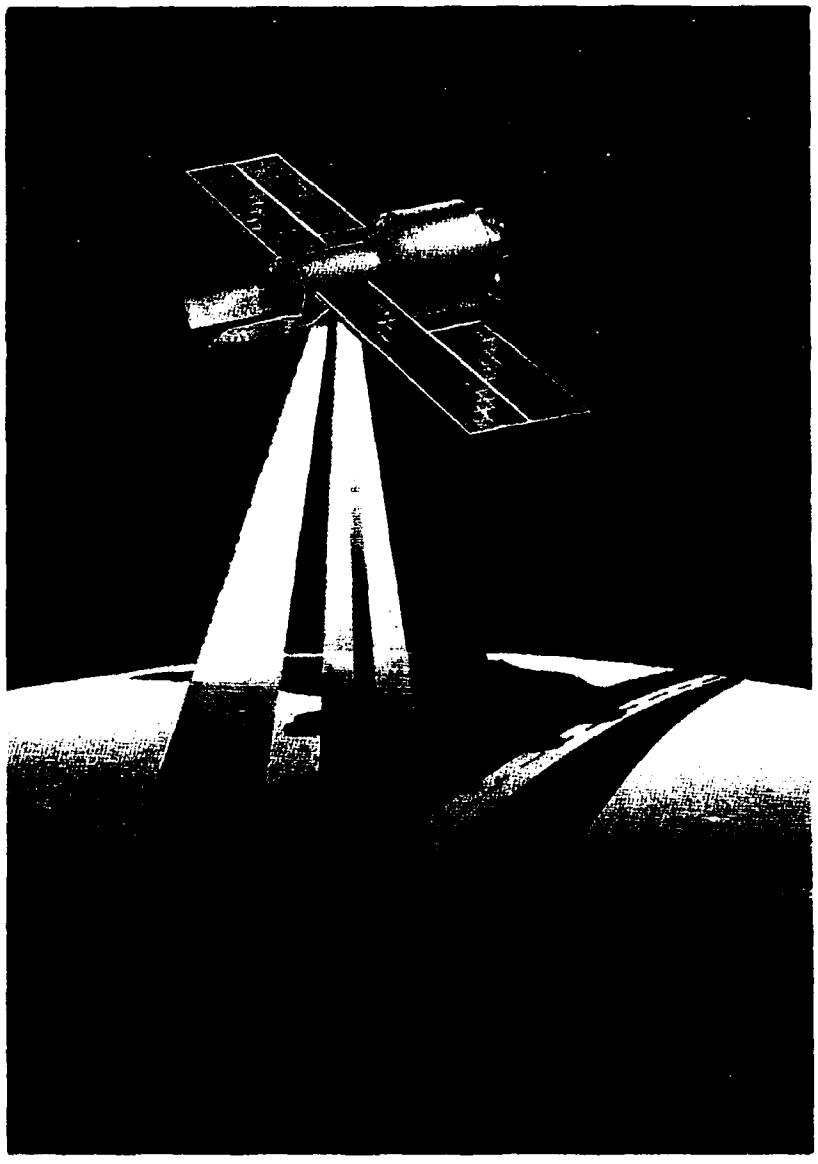

Figure 12: Artist's Impression of ALMAZ in Orbit

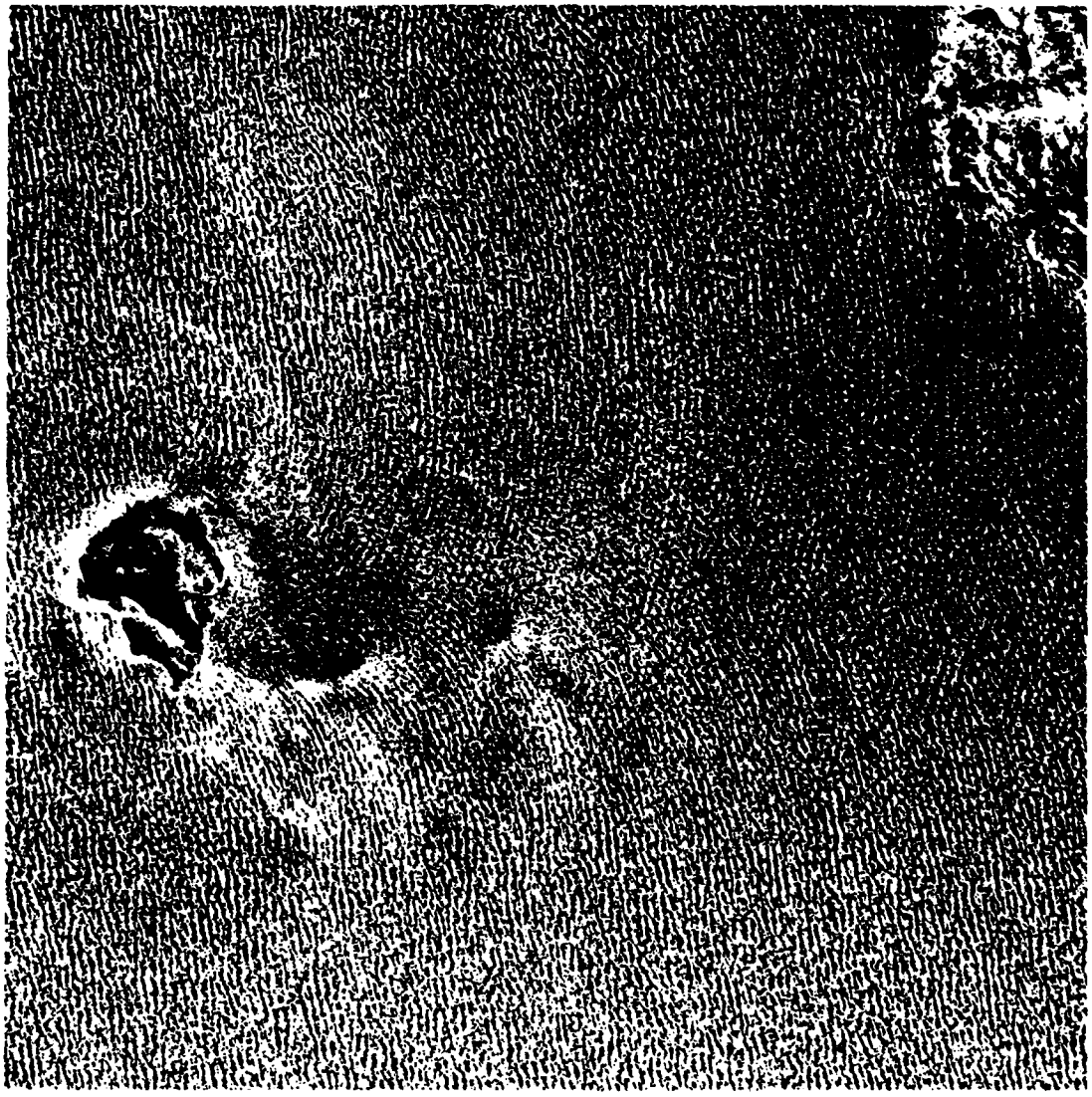

Figure 13: SEASAT Image Showing Surface Waves around Foula

Figure 14: COSMOS-1870 Image of Bushire

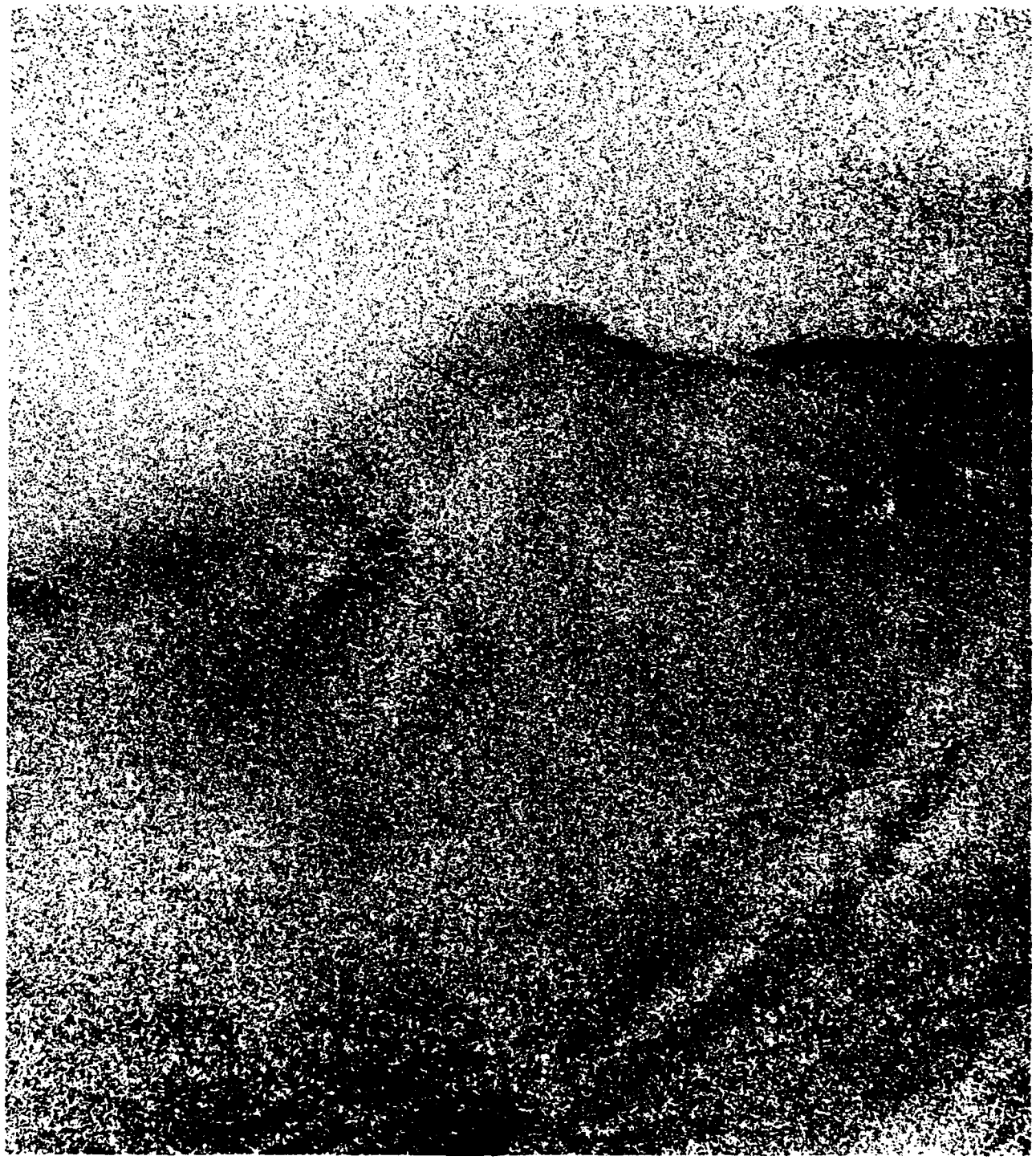

Figure 15: SEASAT Image of the English Channel

Figure 16: SEASAT Image of the Mediterranean Sea, South of Monaco

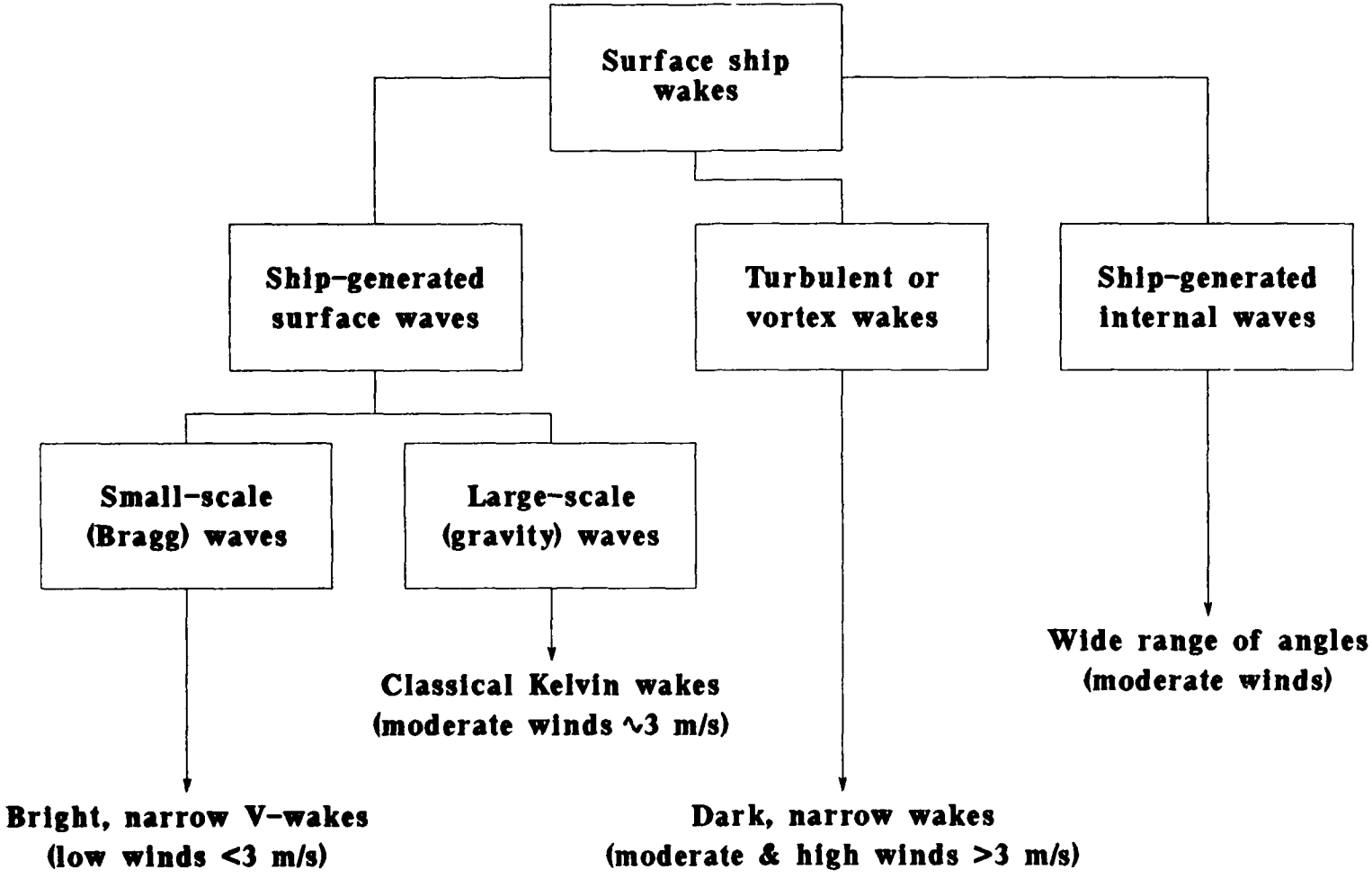

FIGURE 17: Summary of Ship Wake Generation Mechanisms

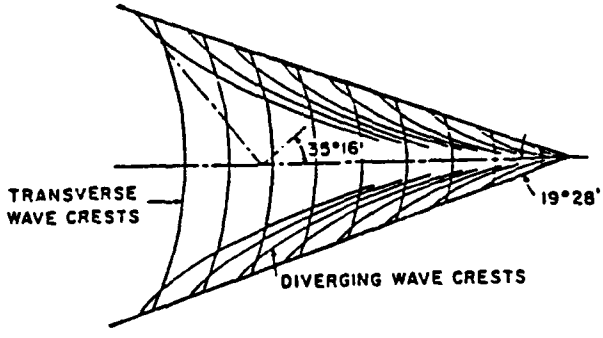

Figure 18: Geometry of the Kelvin Wake

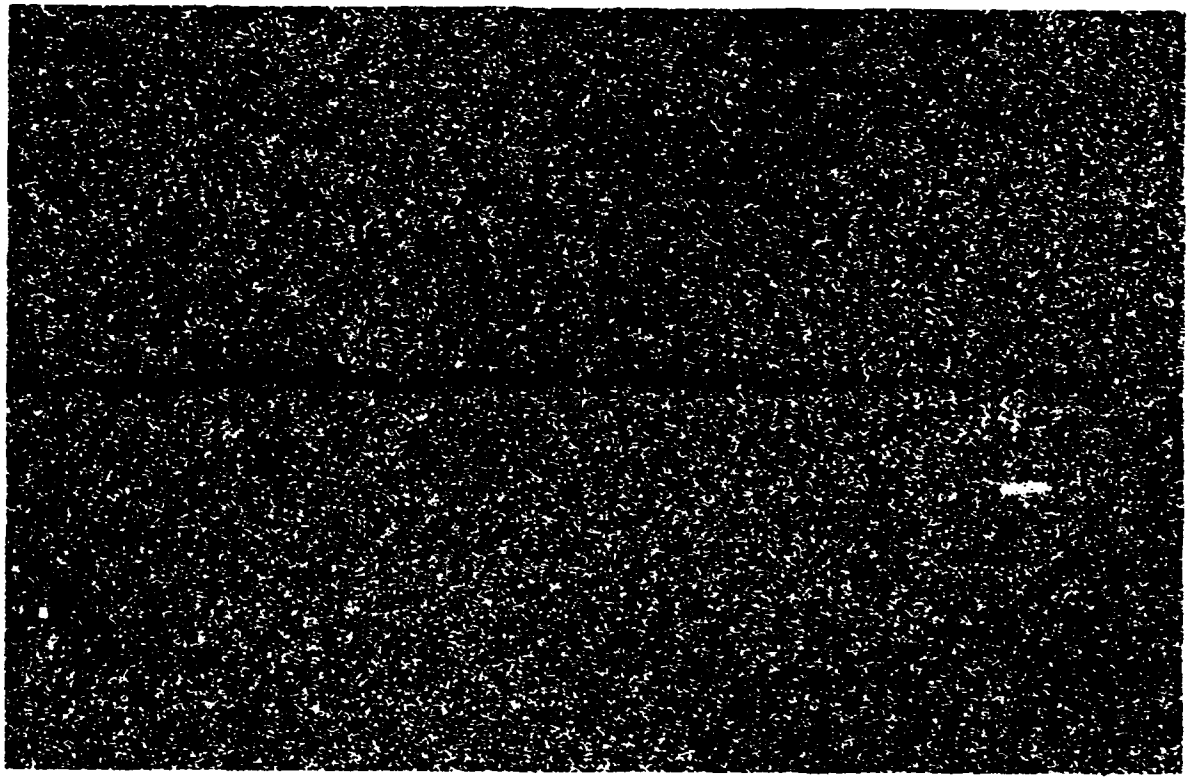

Figure 19: SEASAT In ıge of a Bulk Carrier

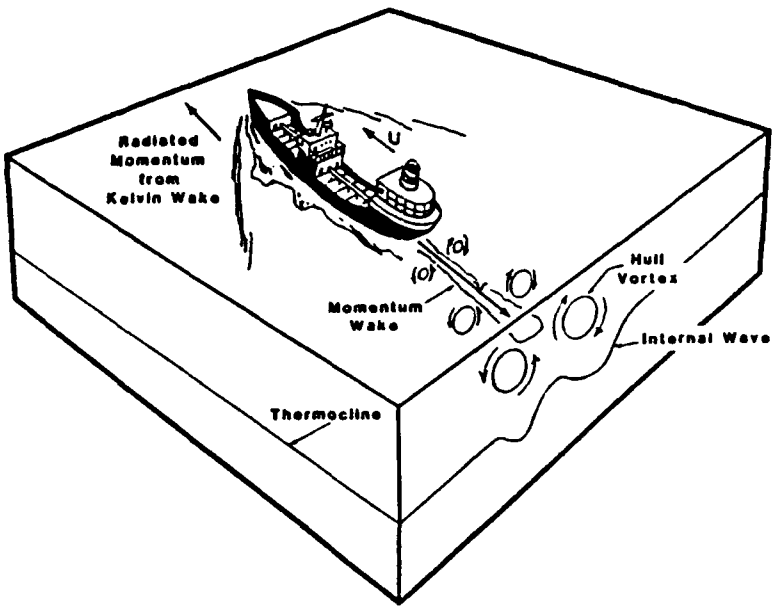

Figure 20: Wake Flow of a Ship

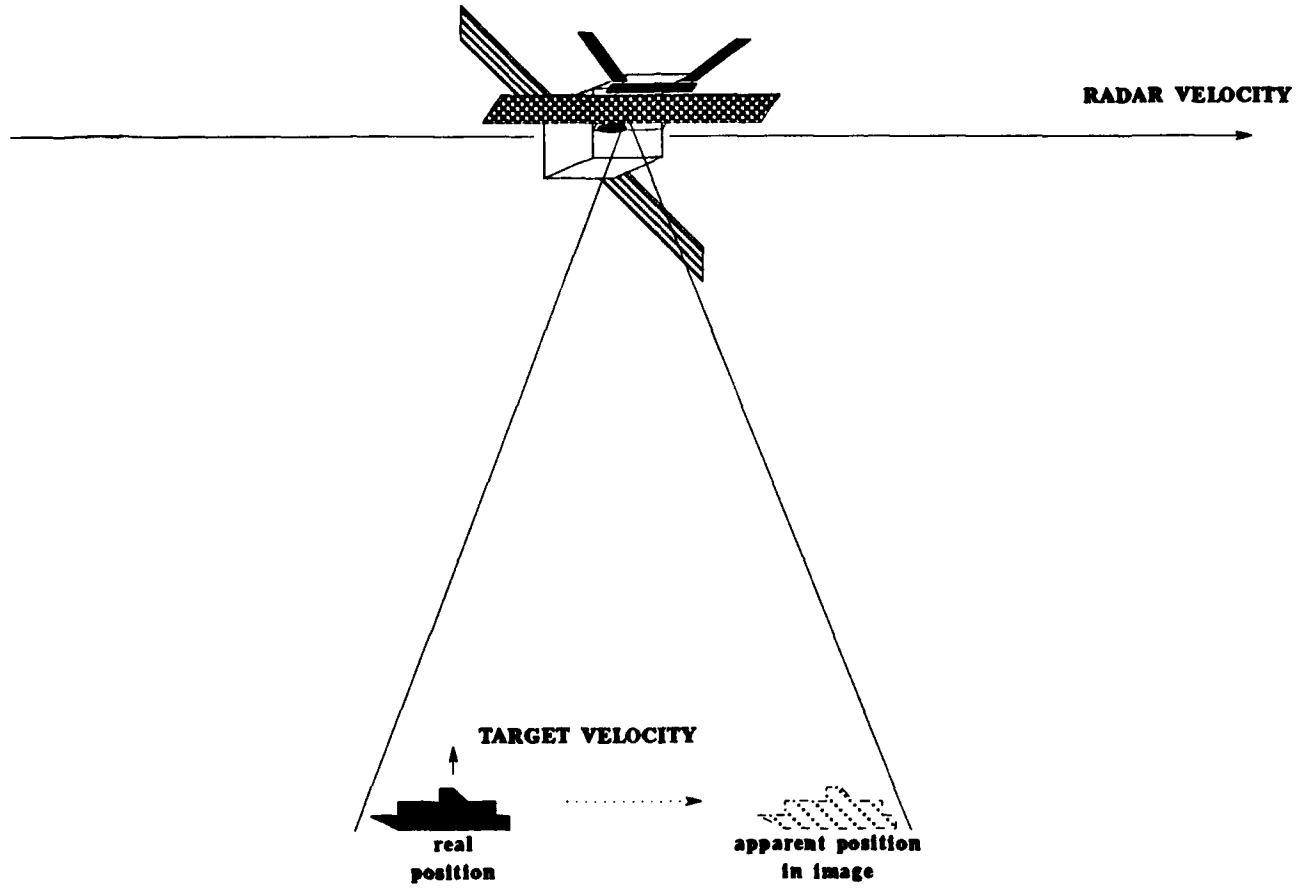

FIGURE 21: Influence of Target Velocity on its Position in the Radar Image

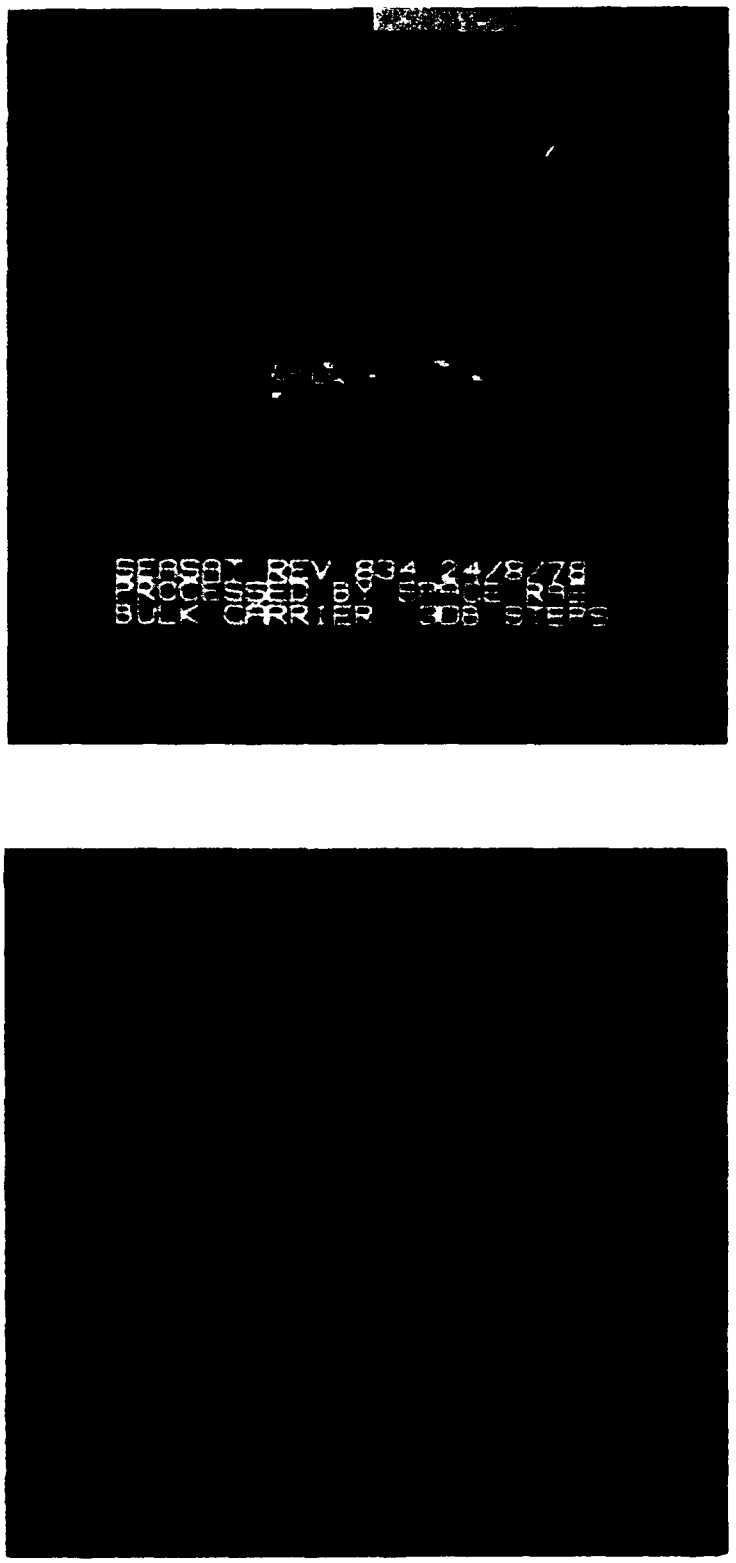

Figure 22: SAR Image of a Bulk Carrier Ship

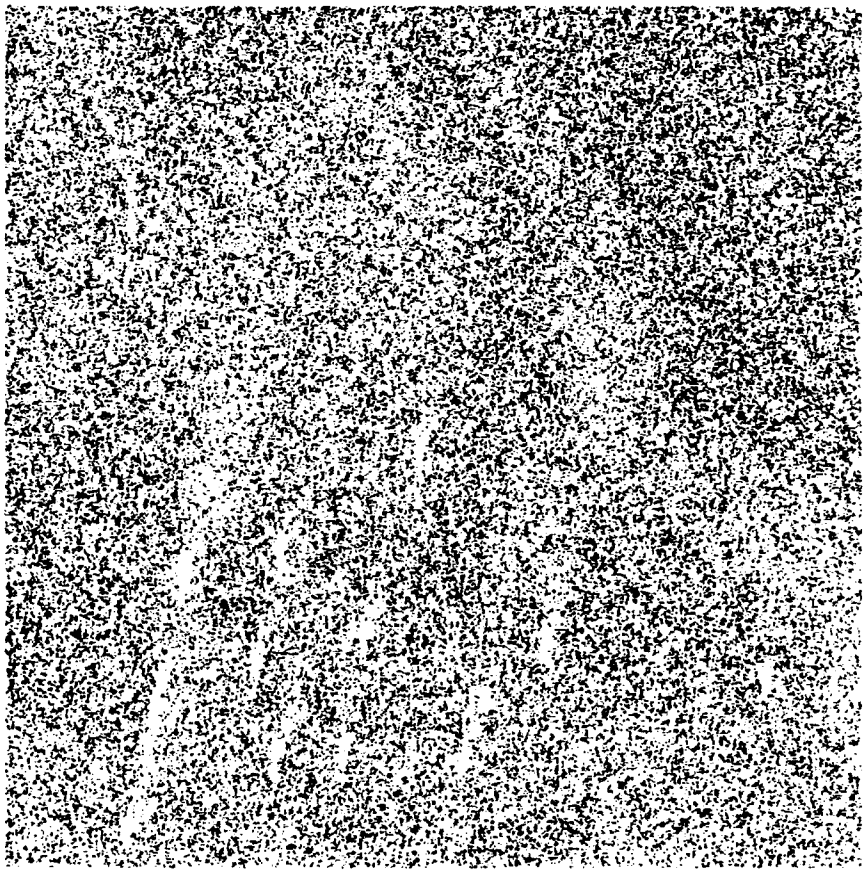

Figure 23: SEASAT Image of an Atlantic Convoy

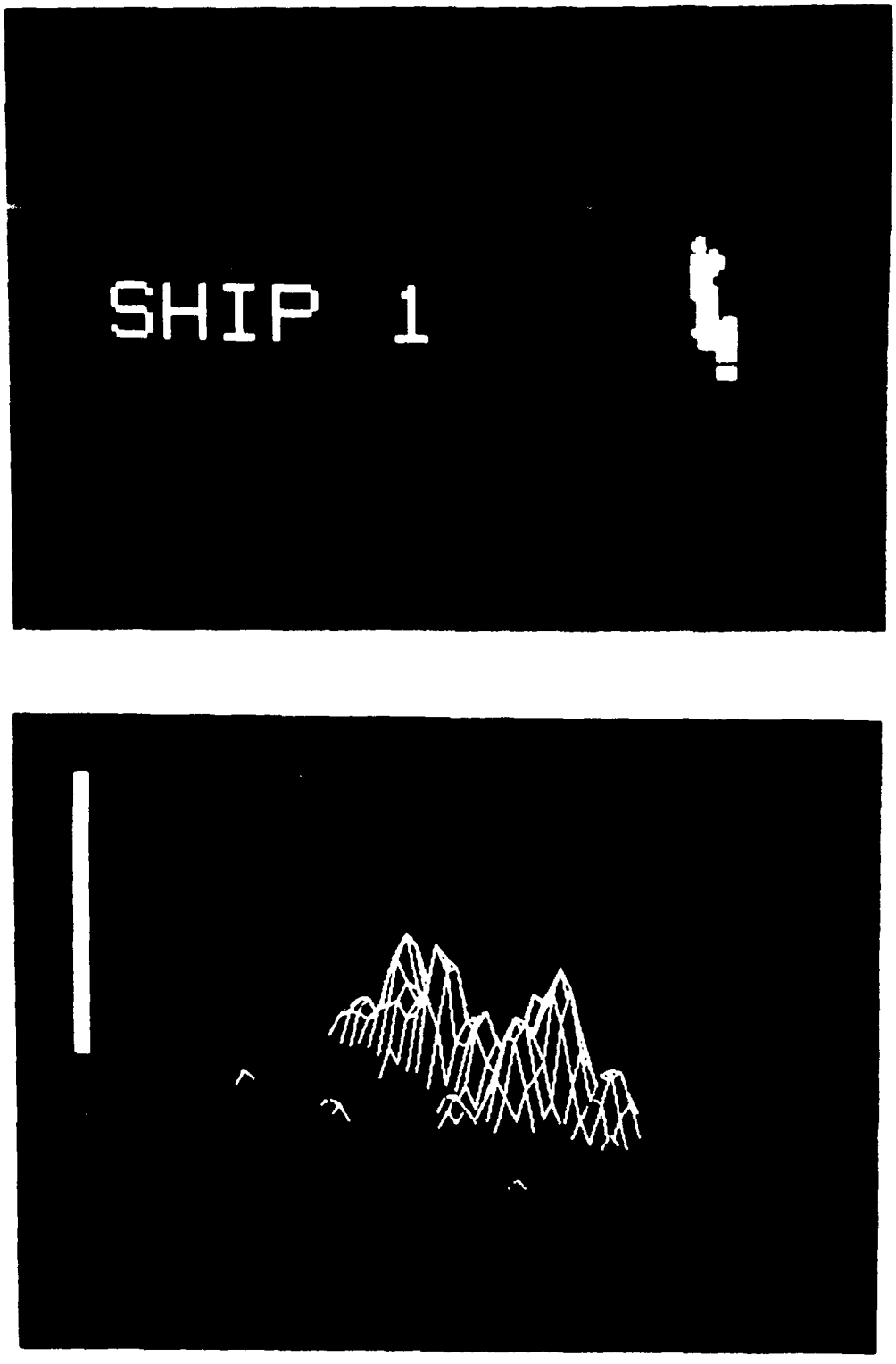

Figure 24: Close-up and 3-D Plot of Central Ship

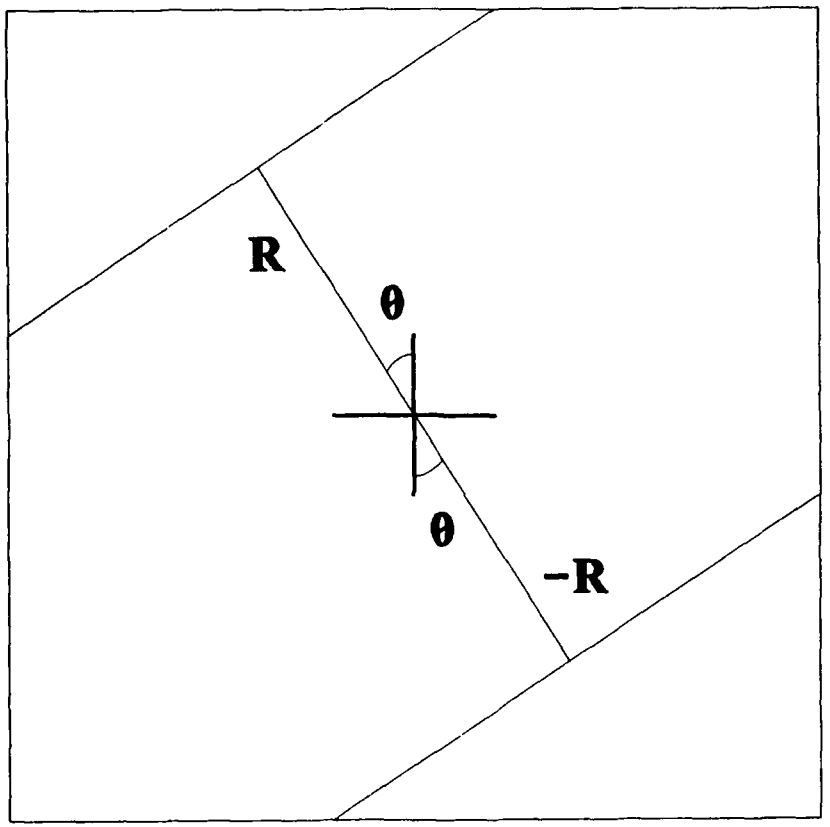

FIGURE 25: The Hough Transform Co-ordinate Scheme

Figure 12: Artist's Impression of ALMAZ in Orbit

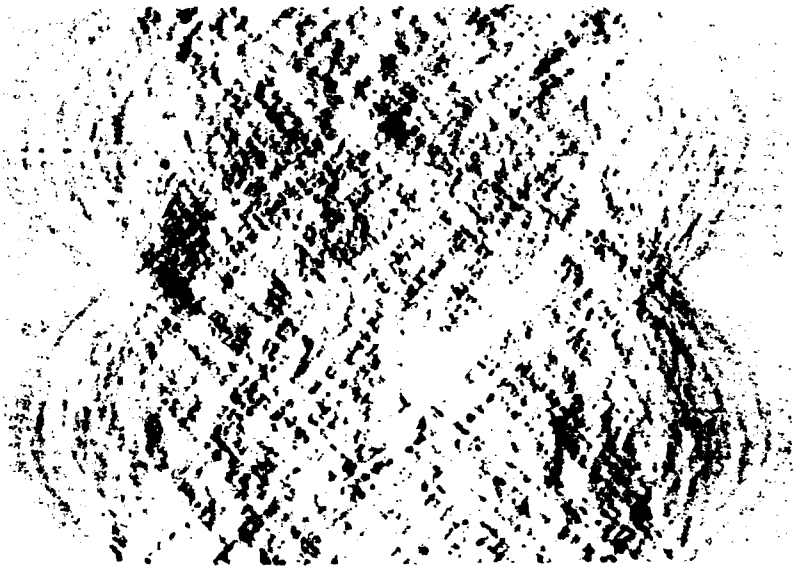

Figure 26: Hough Transform of SAR Ship Wake Image

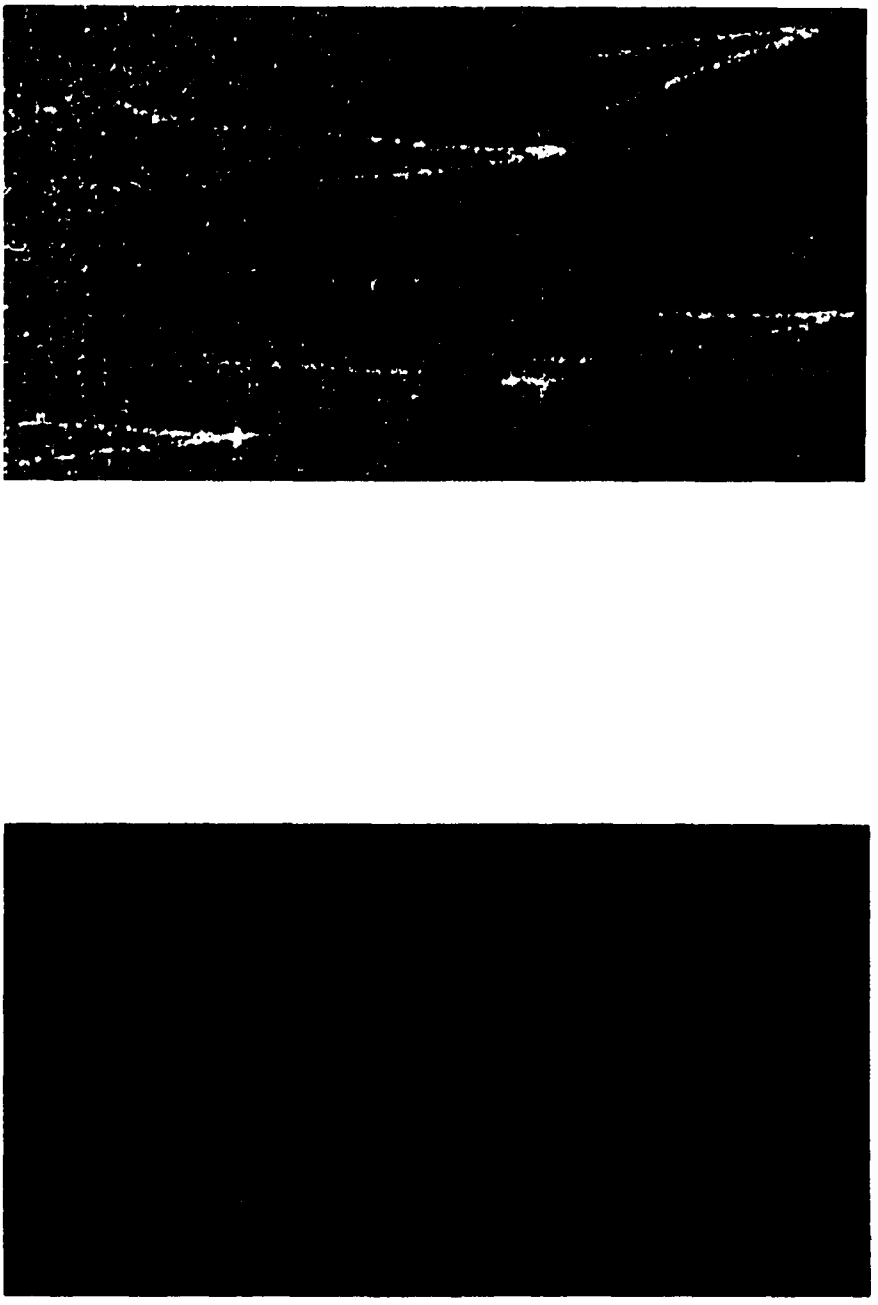

Figure 27: Results of Automatic Ship Wake Detection

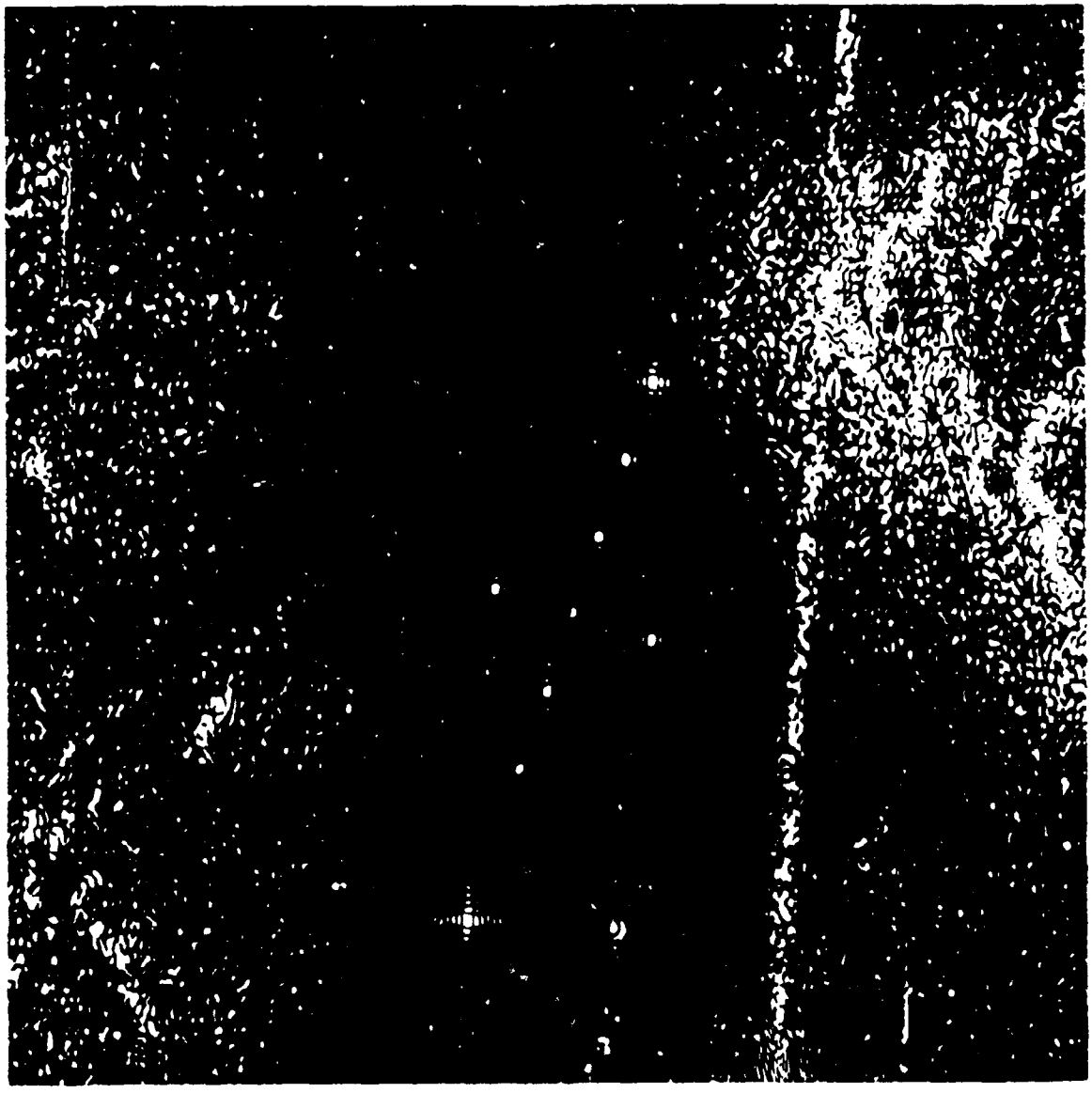

Figure 28: SEASAT Image of Goldstone Corner Reflectors

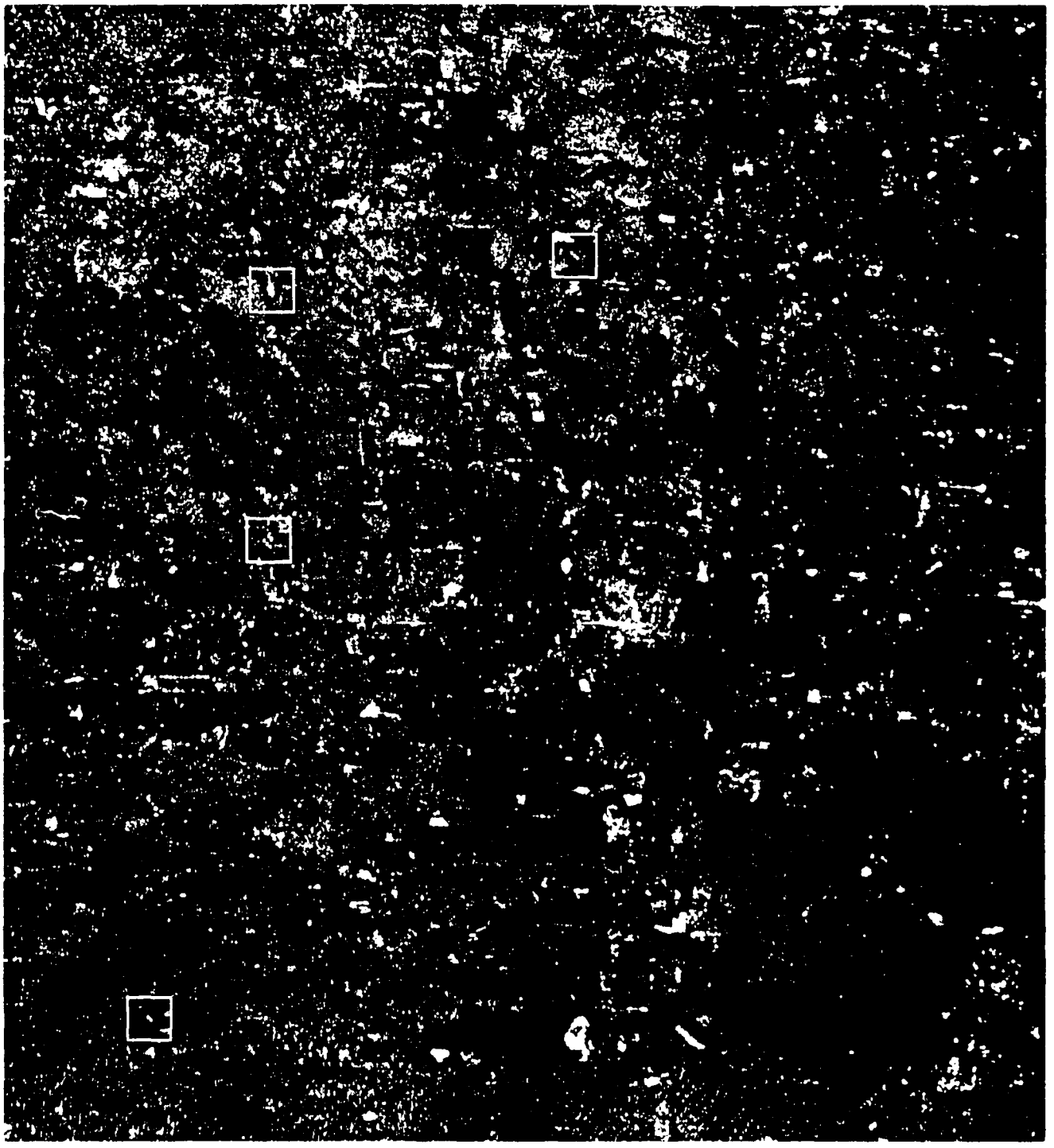

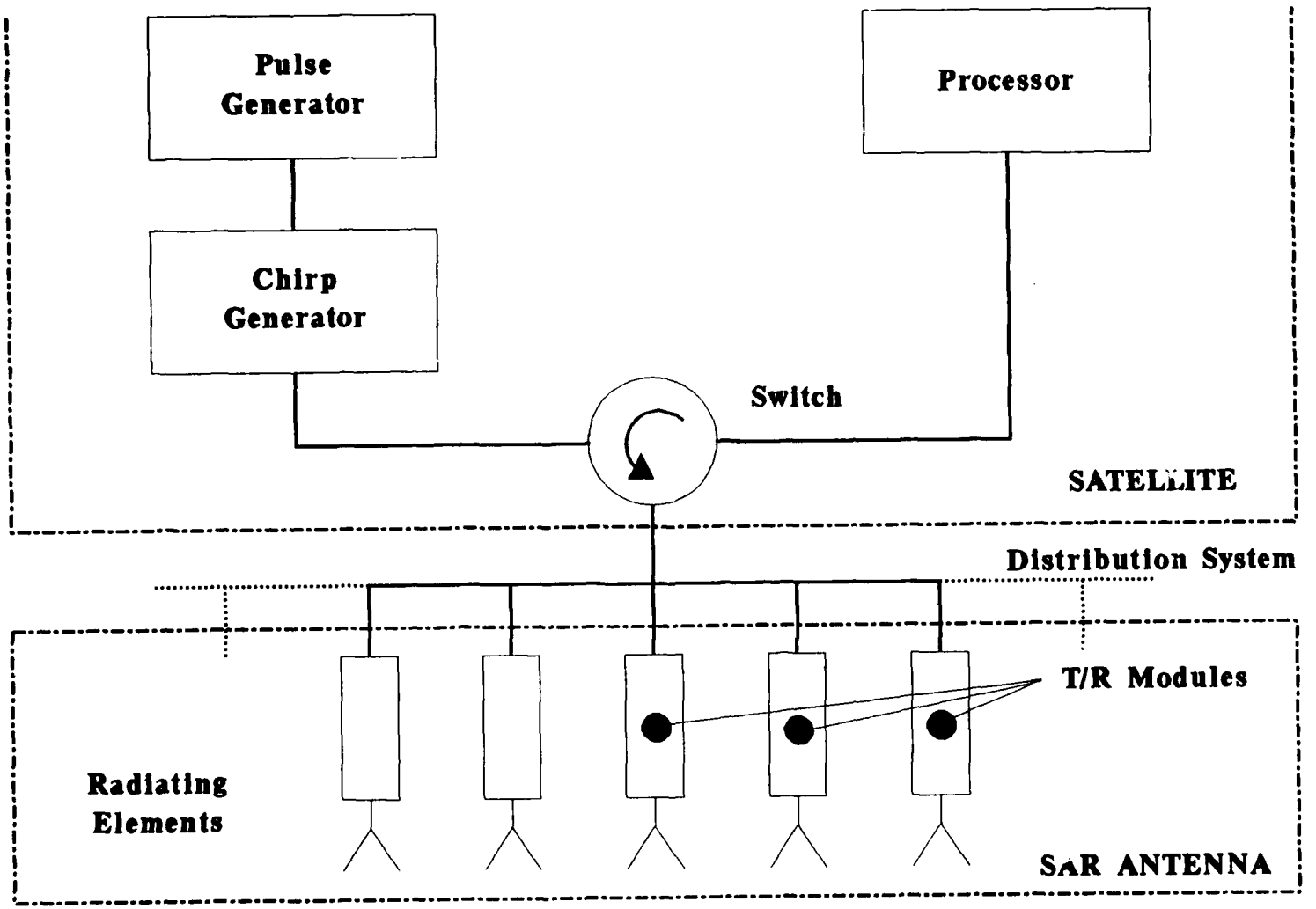

FIGURE 30: Distributed SAR System

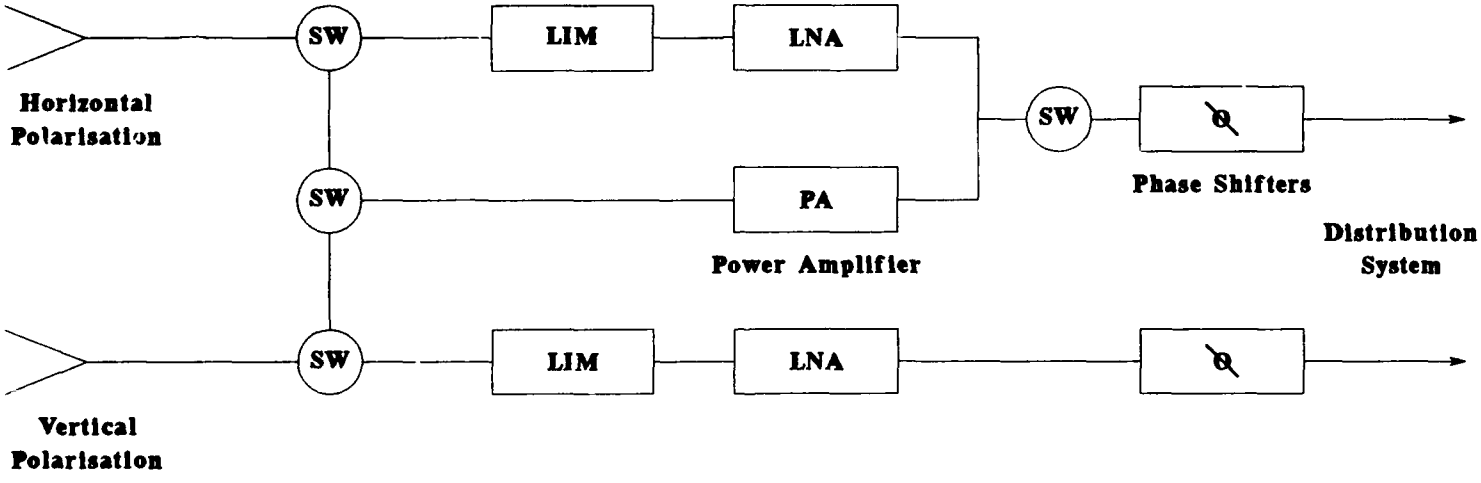

FIGURE 31: Schematic of T/R Module

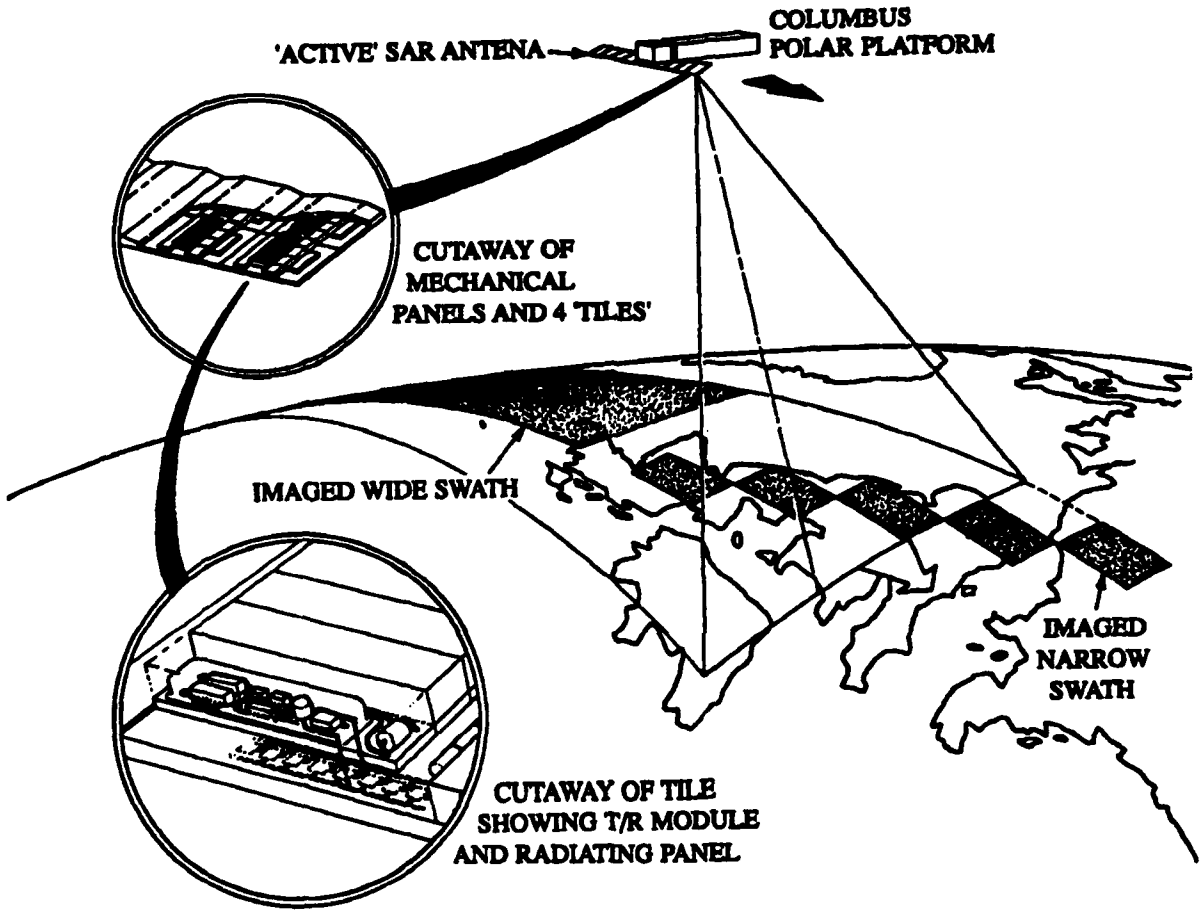

Figure 32: VSAR Instrument Concept

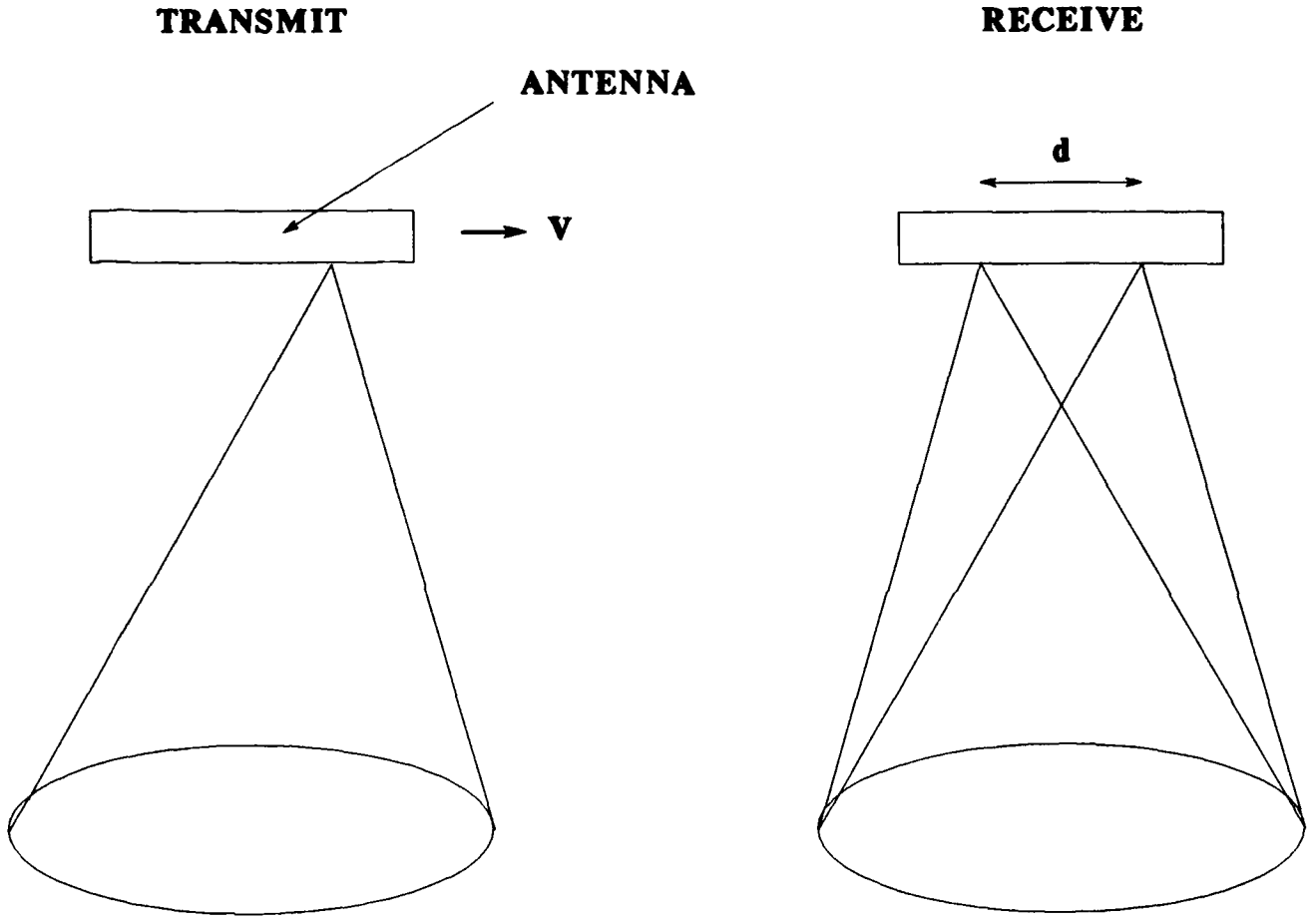

FIGURE 33: Multiple Phase Centre System

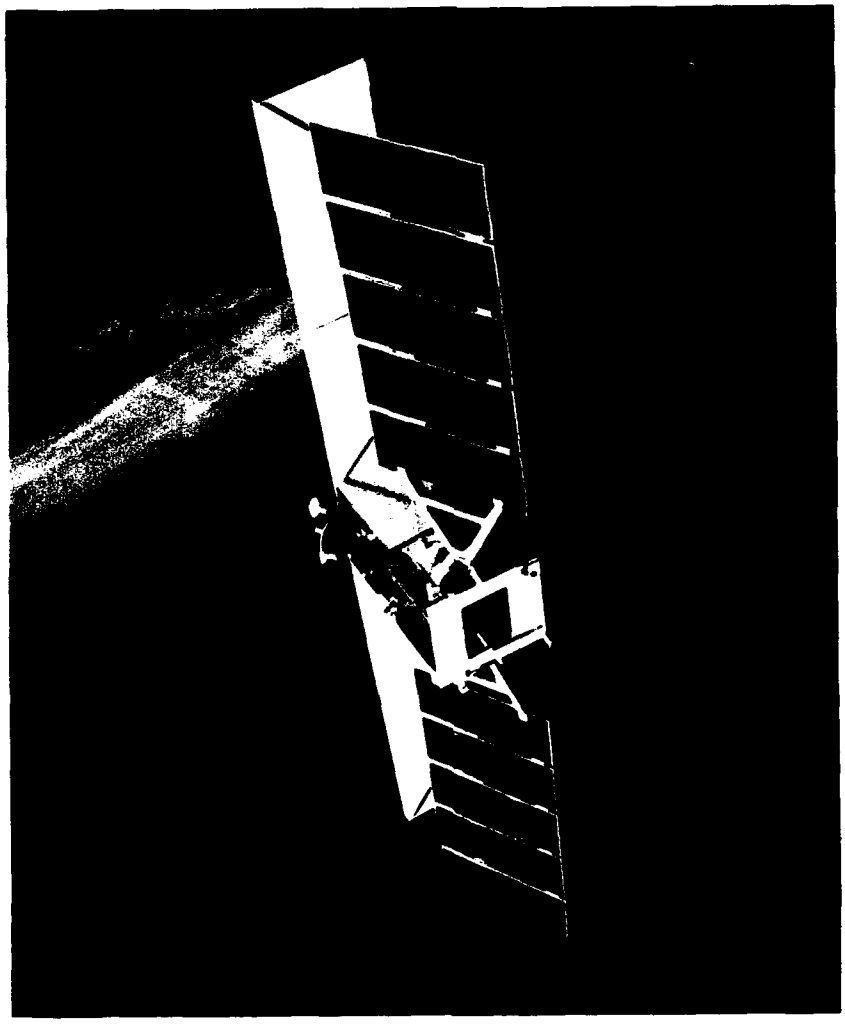

Figure 34: Artist's Impression of RADARSAT in Orbit

Figure 35: ERS-1 First SAR Image

REPORT DOCUMENTATION PAGE

Overall security classification of sheet UNCLASSIFIED

(As far as possible this sheet should contain only unclassified information. If it is necessary to enter classified information, the field concerned must be marked to indicate the classification eg (R),(C), or (S).)

Originator's Reference/Report No DRA TM (AWE) 91013	Month October Year 1991
Originator's Name and Location DRA Portsdown	
Monitoring Agency Name and Location	
Title: The Application of Synthetic Aperture Radar in the Maritime Environment	
Report Security Classification UK UNCLASSIFIED UNLIMITED	Title Classification (U,R,C or S) U
Foreign Language Title (In the case of translations)	
Conference Details	
Agency Reference	Contract Number and Period
Project Number	Other References
Authors: C. J. Condley	Pagination and Ref: 60 / 44

Abstract

A review of the principles of spaceborne Synthetic Aperture Radar (SAR) is given, and its applicationin the maritime environment discussed, with reference to several specific systems. The requirement for calibration is discussed, as are some of the more advanced techniques expected to be incorporated in future missions. The paper was written as a dissertation submitted in partial fulfillment of the requirements for the award of an MSc degree in Microwave Solid State Physics in the Department of Applied Physics and Physical Electronics, University of Portsmouth.

	Abstract Classification (U,R,C or S) U
Descriptors: Synthetic Aperture Radar, SAR	
Distribution Statement (Enter any limitations on the distribution of the document)	